Canadian Mineralogist
Vol. 27, pp. 457-482 (1989)

CHARACTERIZATION OF PHASES AND TWINS IN ALKALI FELDSPARS BY THE X-RAY PRECESSION TECHNIQUE

CATHERINE R. McGREGOR* AND ROBERT B. FERGUSON
Department of Geological Sciences, University of Manitoba, Winnipeg, Manitoba R3T 2N2

ABSTRACT

A procedure is described for rapidly determining, by the technique of single-crystal X-ray precession, the phase, twinning and interphase boundary character of alkali feldspars; the approach is illustrated by representative photographs of specimens of granitic and pegmatitic K-feldspar and albite from Lac du Bonnet, southeastern Manitoba and Dryden, northwestern, Ontario. The possible phases are monoclinic 'orthoclase', microclines of different triclinicities, and albite, any phase occurring either alone or predominant, with another in minor amount. Any triclinic phase may be untwinned, albite-twinned, pericline-twinned or both (*M*-twinned). The boundaries between twinned individuals of one triclinic phase or between K-feldspar and albite phases may be sharp (incoherent) or transitional (coherent). Comparisons are made between effects (*e.g.*, inter-reflection streaking) observable by precession photography and by electron diffraction, as described in the literature. Possible interpretations of other precession effects are suggested by means of diagrammatic lattice models. Comparisons also are made between those features observable on powder records with those on the precession photographs. Answers to questions such as the meaning of some precession effects and how representative the results are of a rock mass, must precede the significant contribution of the method to petrogenesis.

Keywords: X-ray precession, alkali feldspar, orthoclase, microcline, albite, albite twin, pericline twin, powder diffraction.

SOMMAIRE

Nous décrivons une procédure à suivre pour déterminer rapidement par diffraction X (méthode de précession d'un cristal unique) la nature des phases, les macles qui sont développées, et la nature de l'interface entre les phases; nous illustrons la méthode au moyen de photographies représentatives de cristaux de feldspath potassique et d'albite provenant de massifs granitiques et pegmatitiques de Lac-du-Bonnet, au Manitoba et près de Dryden en Ontario. Le feldspath est soit monoclinique ("orthose"), soit triclinique (microcline à triclinicité variable ou albite), chaque phase étant seule ou avec une autre en proportion moindre. Chaque phase triclinique est soit sans macle, ou maclée (selon la loi de l'Albite ou du Péricline, ou montrant une répartition "*M*" de domaines maclés selon les deux lois). Le passage d'un domaine à un autre dans une macle d'une phase triclinique ou d'un domaine potassique à un domaine sodique dans une perthite peut être franc (interface noncohérente) ou transitionnel (interface cohérente). Nous comparons les observations faites sur un cliché de précession, par exemple les taches étirées, et leurs analogues en diffraction électronique, telles que décrites dans la littérature et interprétées par microscopie électronique par transmission. Des interprétations possibles d'autres effets de précession sont présentées au moyen de modèles idéalisés du réseau. Nous comparons aussi les clichés de précession et ceux que l'on obtient par la méthode de poudres. Une détermination définitive de la cause de certains effets de précession et une étude de la représentativité des résultats à un massif entier doivent précéder l'application de ces observations aux questions pétrogénétiques.

(Traduit par la Rédaction)

Mots-clés: diffraction X, méthode de précession, feldspath alcalin, orthose, microcline, albite, macle de l'Albite, macle du Péricline, méthode des poudres.

INTRODUCTION

X-ray *powder* diffraction has long been used to characterize the assemblage of alkali feldspars in a rock, whereas *single-crystal* techniques have rarely been used for this purpose, presumably because the method is less straightforward and because the results (*e.g.*, twin character) are not so readily interpreted in petrogenetic terms as those from powder diffractometry (*e.g.*, refined cell-parameters). However, some crystallographic characteristics observable only by single-crystal techniques, such as albite–pericline twinning, are of potential petrogenetic value; in this paper, we spell out the precession technique, the most widely used of the photographic single-crystal techniques, as it applies to the alkali feldspars. Some precession effects (*e.g.*, reflection streaking) are more or less comparable to those obtained by electron diffraction, and a comparison of these effects as described in the literature is given later in the paper.

The precession investigation of a 'single' crystal can provide information on (1) character of the phase(s) present, maximum (low) microcline, intermediate microcline(s), monoclinic K-feldspar ('orthoclase'), and Na-rich plagioclase ('albite'), or a combination of these; (2) the twin character of microcline and albite, which may be untwinned, albite-twinned, pericline-twinned, or albite- and pericline- (*M*-) twinned; (3) tricinicity of the microcline phase(s); and (4) nature of interdomain

*Present address: Manitoba Department of Energy and Mines, 555-330 Graham Avenue, Winnipeg, Manitoba R3C 4E3.

(phase or twin-component) boundaries, either sharp (incoherent) or transitional (coherent).

Interpretations of the precession photographs were enhanced by taking Gandolfi powder-type photographs of the same crystal, and powder diffractograms of the same bulk sample. Electron-microprobe chemical analyses also were made of the same crystal, and results of partial chemical analyses of the bulk samples were available to the authors.

Specimens and Sample Selection

The precession photographs described here pertain to fourteen specimens of alkali feldspar: one of 'orthoclase' (monoclinic adularia), eleven of microcline and two of albite (Table 1). The microcline and albite specimens are part of a suite of 31 described by McGregor (1984) ; they were provided by Petr Černý, who documented the geological setting and provided geochemical data. They are from Precambrian granitic and pegmatitic rocks from Lac du Bonnet, Manitoba and Dryden, Ontario. The adularia is from Fierstal, Switzerland (University of Manitoba Mineralogy Museum, no. 313-3).

Two points must be made about the description that follows. First, although many if not most 'single crystals' ($> \sim 0.1$ mm) of alkali feldspars are either twinned aggregates or lamellar intergrowths of two or more feldspar phases, or both, the technique described here for investigating them is the single-crystal precession; thus in the following

TABLE 1. SOURCE AND CHEMICAL DATA FOR THE ALKALI FELDSPAR SPECIMENS[1]

feldspar name[2]	specimen identifier	source		microprobe comp'n., mol.%[4]			
		locality[3]	rock type	Or	Ab	An	Other
OR	adularia no. 313-3: MONO	(3)	unknown	92.9	7.1	--	--
MM[5]	AEC-20	(1)	hbl. bio. tonalite	90.8	7.9	--	Cn 1.3
	APG-05	(2)	pegm. granite	90.1	8.5	0.7	Rb-f 0.5 Cs-f 0.1
	CG-03	(2)	grano-diorite	91.0	6.9	--	Cn 2.1
	GPE-11	(2)	pegmatite	85.2	6.5	0.9	Rb-f 6.2 Li-f 0.7 Cs-f 0.6
	MLG-01	(2)	grano-diorite	94.5	5.5	--	--
	MLP/NZ-24	(2)	pegmatite	86.7	5.5	1.0	Rb-f 5.1 Li-f 1.2 Cs-f 0.1
	PG-24	(1)	biotite granite	89.6	10.4	--	--
	PG-121	(1)	leuco-granite	93.6	6.4	--	--
	PG-133	(1)	biotite granite	not analyzed			
	SR-97	(1)	porph. hbl. bio. granodi.	92.8	5.0	--	Cn 2.2
	SR-148	(1)	porph. hbl. bio. granodi.	93.1	6.9	--	--
LA	CG-03AB	(2)	grano-diorite	not analyzed[6]			
	PG-138AB	(1)	hbl. bio. tonalite	not analyzed[6]			

[1] Note: (a) Data from McGregor 1984, text pp. 13-19 and Tables 4-2 and 5-1. (b) For interrelation of specimen and figure numbers, see Table 2 and for derived crystallographic data, Table 5. [2] OR orthoclase, MM maximum microcline, LA low albite. [3] (1) Lac du Bonnet, Manitoba; (2) Dryden, Ontario; (3) Fierstal, Switzerland. [4] Note: (a) Electron microprobe by McGregor supplemented in some cases by wet chemical analyses by Ukacuwun (1981) for one or more of Ca, Rb, Cs on bulk powdered samples of the same specimen (see McGregor 1984, Table 4-2 for details). (b) For estimated amounts of separate-phase albite, see Table 5. [5] Note: (a) MLP/NZ-24 also contains intermediate microcline. (b) Most specimens contain minor separate-phase albite (see Table 5). [6] Refined unit-cell parameters (McGregor 1974, Table 3-7) are close to those for low albite.

description the fragment being subjected to precession investigation is referred to as a 'crystal' regardless of its possible twinned or intergrowth character.

The second point is that maximum microcline is used (mainly) to illustrate the detailed procedure because crystals of microcline are in general more complex than those of the other alkali feldspars. However, characteristic precession photographs of low albite also are given.

For this procedure, a crystal or, more usually and preferably, a fragment showing the nearly perpendicular {010} and {001} cleavages, ~0.1–0.5 mm in size, is picked from crushed material under the microscope. Coarse material from pegmatites presents no problem (Ucakuwun 1981), but for finer-grained material from granites or gneisses, we have found it desirable to use the following technique (Van der Plas 1966, Kaneko 1974): (1) the rock sample is crushed for a few seconds in a 'shatterbox'; (2) the crushed sample is sieved to give a fraction larger than 0.5 ϕ (0.71 mm); (3) the sieved grains are disseminated on a flat surface, and etched in HF vapor for

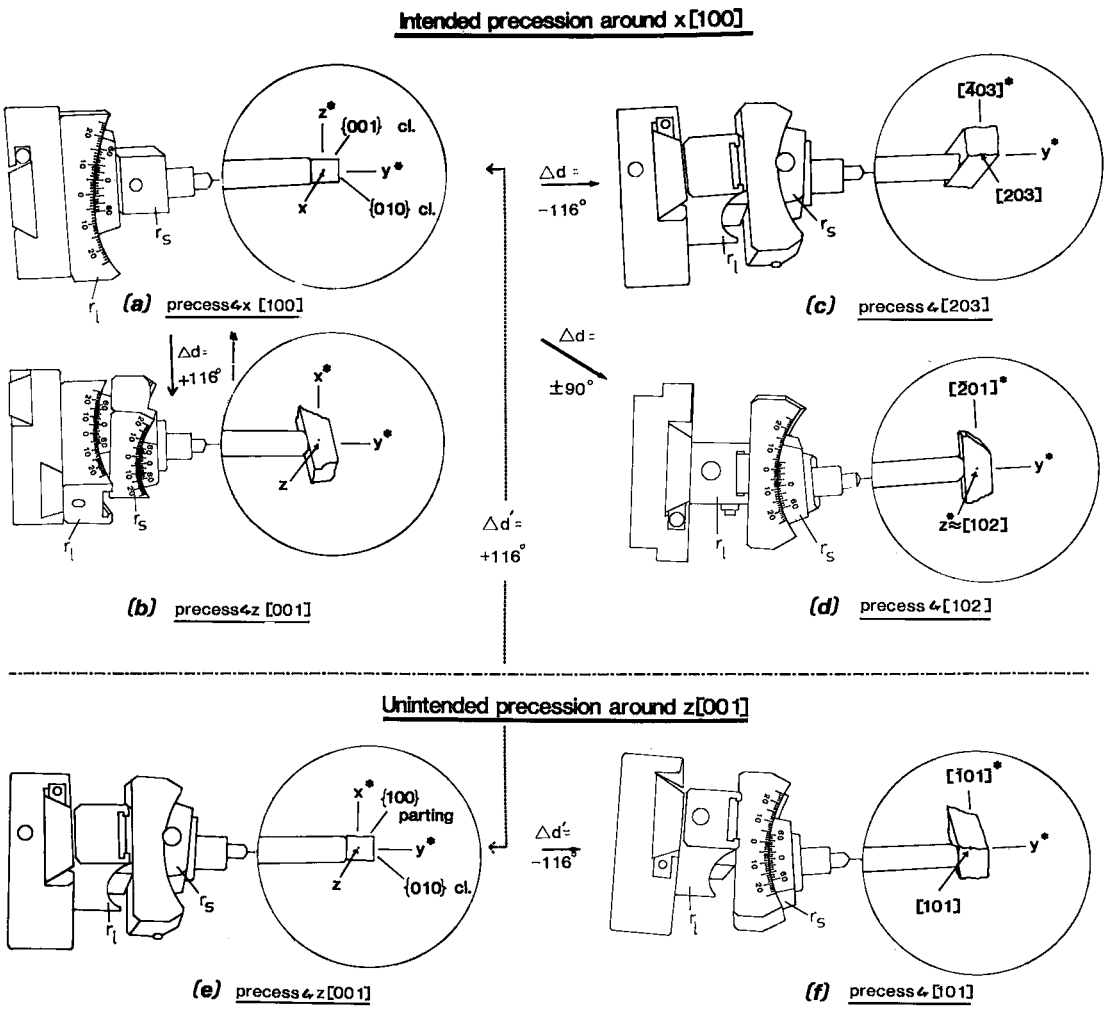

FIG. 1. Rotation positions of the crystal on the goniometer head in relation to the orientation procedure described in the text. Within the circles, the crystal and glass rod are greatly enlarged for clarity. In all sketches, the precession axis and the X-ray beam are normal to the plane of the drawing. Designations: r_s small rocker (arc). r_l large rocker (arc), Δd change in the dial reading. It is arbitrary whether the X axis (parallel to the two cleavages) is initially set parallel to r_s or to r_l; in this example it is the former (easily seen in a or d). The signs of Δd shown here also are arbitrary, but they must all be the same as, or the reverse of, those shown. This Figure relates particularly to the photographs in Figures 2 and 4, and to the diagrams in Figure 3.

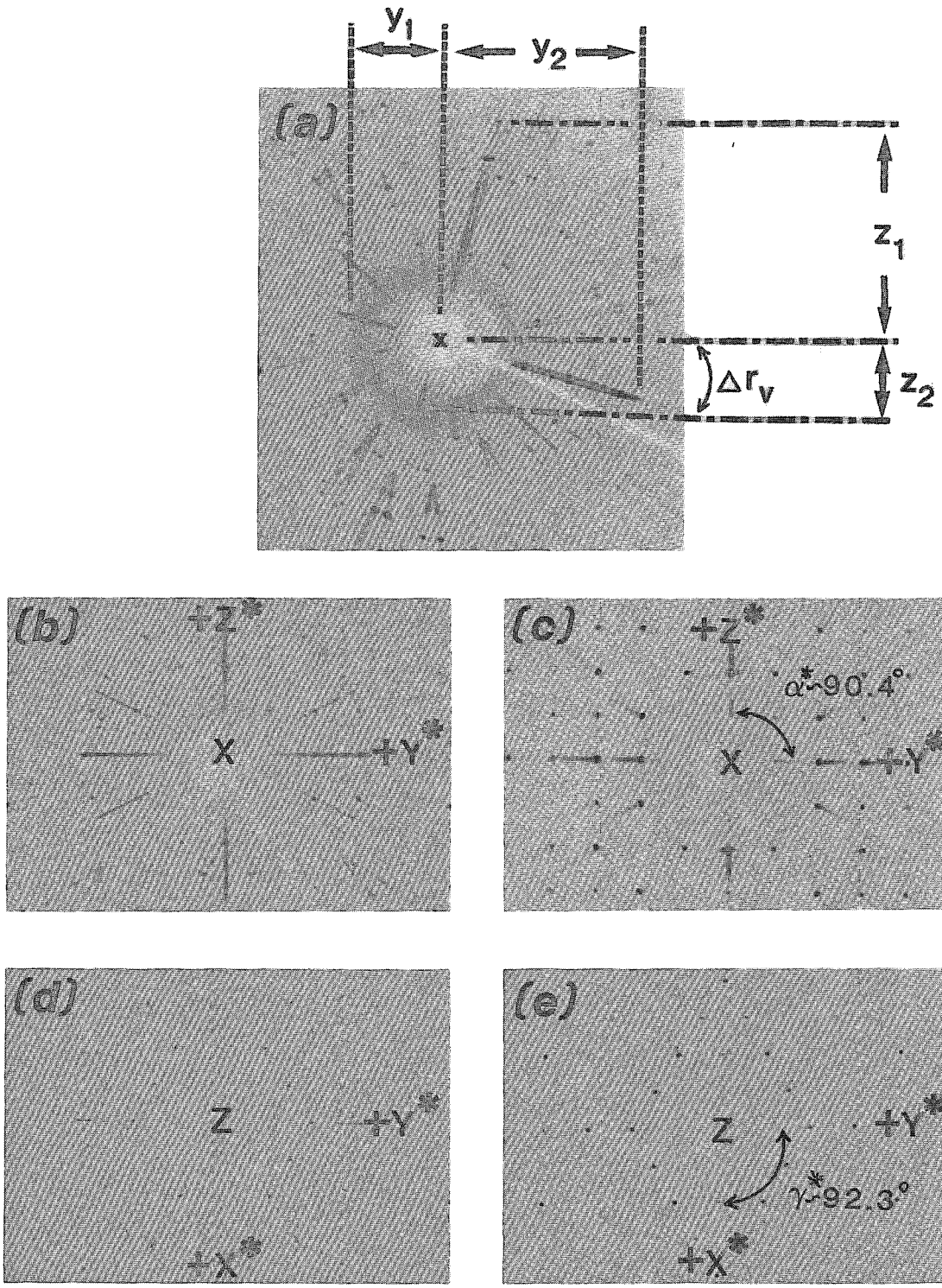

FIG. 2. Setting and 0-level precession photographs to scale of untwinned maximum microcline around the *X* and *Z* axes; rotation axis (horizontal) is *Y**. Experimental conditions: for all photos, crystal-to-film distance F = 60.0 mm; for

15 minutes; (4) the etched grains are immersed in a solution of sodium cobaltinitrite for one minute; and (5) appropriate fragments of yellow-stained K-feldspar or unstained Na-feldspar are selected manually under the microscope. (On stained crystals, the small volume and polycrystalline character of the stain preclude discernible precession effects.)

Precession Photography: Procedures

The precession method and the concept of the reciprocal lattice essential to the interpretation of precession photographs are described in such crystallography texts as Henry *et al.* (1960), Nuffield (1966) and Azaroff (1968), and in the book devoted to the method by Buerger (1964). For the application of the method to the feldspars, the description in Smith (1974, Chapter 6) is essential reading (see also Smith & Brown 1988, pp. 121-128); the description given below assumes that the reader is familiar with Smith's account.

In the description that follows, X, Y, Z and X^*, Y^*, Z^* denote axial *directions* whereas a, b, c and a^*, b^*, c^* denote axial *periods* (repeat distances along the axes).

Selecting and mounting the crystal

(a) The fragment chosen must show, for rapid orientation, two faces or, as is usual, cleavages at ~ 90°, presumed to be {010} and {001} (Figs. 1a–d). The fragment should be nearly equidimensional; it is important to note that if it is larger than ~ 0.5 mm, important detail on the precession photographs may be obscured.

(b) Under crossed polars the optical extinction angles on the two planes are measured to confirm the identity of the crystal, and to differentiate the two cleavages as {010} or {001} using the following relevant extinction angles (Smith & Brown 1988, p. 186, where the primary sources are given; orthoclase data from Tuttle 1952):

	Resting on {010},°	Resting on {001},°
maximum microcline	5	18
orthoclase	~ 5	0
high sanidine	5	0
low albite	20	3
high albite	8	8

(c) Under the binocular microscope, the crystal is mounted on a fine glass rod normal to {010} (Figs. 1a–d, enlargements) using an adhesive such as vaseline; the glass rod itself is mounted on a brass pin held in the goniometer head.

(d) The brass pin is rotated in the head until {001} is approximately parallel to either the small or large rocker (or arc) (Figs. 1a,d, small rocker r_s), the locking screw tightened, and the head mounted on the precession instrument. The crystal will then be *rotating* approximately about the normal to {010}, *i.e.*, the Y^* axis.

The objective at this stage is to orient the crystal for precise *rotation* around Y^*, and precise *precession* around the direct X axis, which involves setting the edge between {010} and {001} ($=X$) parallel to the X-ray beam when the instrumental precession angle μ is at 0°.

Orientation procedure exemplified by microcline

Three instrumental settings (all in degrees) are required to achieve the desired orientations of the crystal: (i) the vertical rocker, which controls the tilt of the Y^* rotation axis: setting symbol r_v, correction Δr_v; (ii) the horizontal rocker, which controls the fore-aft position of Y^* in the horizontal plane, and is used to bring X (normal to it) into coincidence with the X-ray beam: r_h, Δr_h; and (iii) the dial (or drum) of the rotation axis, which controls the up-down motion of the precession axis: d, Δd. The magnitudes of the setting corrections Δr_v, Δr_h, Δd are taken from an *orientation photograph* which, when related to the crystal on the instrument, also provides a + or − sense to each correction.

The experimental conditions for orientation photographs are: unfiltered MoK X radiation, *i.e.*, MoK α-β radiation; precession angle μ 10°; crystal-to-film distance F 60.0 mm; no screen; and either a Polaroid Land diffraction cassette with 4″ x 5″ Polaroid Land film, type 57 (ASA 3000) with normal exposure ~5 minutes, or the film cassette of the precession instrument with medical or industrial X-ray film and an exposure of ~1 hour.

The steps in the orientation procedure are as follows:

(a) With μ at 0°, the goniometer head is rotated until an edge between {010} and {001} (*i.e.*, X) is visibly parallel to the X-ray beam direction, in which orientation either the small or large rocker will be vertical, the other horizontal (Fig. 1a, large vertical).

setting photos a, b, d, radiation unfiltered Mo$K\alpha$-β, precession angle μ = 10°, no screen; for 0-level precession photos c. e, Zr-filtered Mo$K\alpha$, μ = 25°, screen radius r = 15 mm, screen-to-crystal distance s = 32.6 mm. (a) Setting X-axis photograph, misoriented; corrections y, Δr_v, *etc.*, explained in the text; (b) setting X-axis photograph, oriented; (c) 0-level precession around X; (d) setting Z-axis photograph, oriented; (e) 0-level precession around Z. Photos a–c are of specimen CG-03; d,e, of PG-121 (Table 2).

TABLE 2. SUMMARY OF ALL SINGLE-CRYSTAL PRECESSION PHOTOGRAPHS AND POWDER DIFFRACTOGRAMS (AS FIGURE NUMBERS) AND CORRELATION WITH SPECIMEN NUMBERS

FELDSPAR PHASE(S)[1]	Precession direct axis -> / Reciprocal lattice plane-> / Twin character †	precession photographs: X[100] Y*Z*	z[001] X*Y*	[203] Y*[$\bar{4}$03]*	[101] Y*[$\bar{1}$01]*	[102] Y*[$\bar{2}$01]*	diffractograms
OR			6(b): MONO	4(a): MONO			12(b): MONO
MM	UNTWINNED		2(d),(e), 6(c):PG-121			4(c): MLG-01	12(c): PG-121
	ALBITE-TWINNED	2(a)-(c): CG-03;	6(d):PG-24; 9(a):CG-03[2] 9(c):SR-97[2]		4(b): PG-133		
	PERICLINE-TWINNED		6(e): SR-148				
	M-TWINNED	6(a): PG-24	6(f):APG-05; 9(d):GPE-11[2]				12(d): GPE-11[2]
MM + OR	ALBITE-TWINNED MM		9(b): MLP/NZ-24[2]				12(e): MLP/NZ-24[2]
LA ONLY	UNTWINNED	7(a),(b): CG-03AB	7(e),(f): CG-03AB				12(a): CG-03AB
	ALBITE-TWINNED	7(c),(d): PG-138AB					
(MINOR) LA WITH MM	UNTWINNED LA	11(a):AEC-20					12(f): CG-03
	ALBITE-TWINNED LA	11(b):CG-03					
	M-TWINNED LA	11(c):SR-97					

[1] Abbreviations as in Table 1. [2] Illustrating streaked or broadened reflections.

Instrumental readings r_v, r_h, d are recorded, and orientation photograph no.1 taken. It will normally be somewhat similar to that for an untwinned microcline, shown as Figure 2a. (For a twinned crystal, refer to Table 2 and see below.)

If the crystal is oriented as desired, the strong quasi-horizontal and quasi-vertical streaks will be, respectively, Y^* containing the ($0k0$), and Z^* the ($00l$), reflections. The labeling of the axes is confirmed by comparison with the photographs in Figure 2, or by measuring (in mm) the reciprocal distance $2p^*$ between pairs of corresponding reflections on these streaks across the center (or p^* from one reflection to the center), and matching the $2p^*$ values and qualitative intensities with those given in Table 3. If there is uncertainty about the identification of the axes at this or the next stage, the crystal should be replaced with another.

(b) The magnitude and sense of the corrections Δr_v, r_h, Δd are now deduced from orientation photograph no.1 (Fig. 2a) (see *e.g.*, Nuffield 1966, p. 266-273) utilizing the displacement from the center of the film of the center of a circle of strong reflections or streak ends (see Figs. 2a,b). These corrections enable one to set X along the X-ray beam and the Y^* Z^* plane normal to the beam at $\mu = 0°$. Correction Δr_v is simply the departure of the quasi-horizontal axis from the true horizontal. Corrections Δr_h and Δd are derived from the differences in the horizontal and vertical streak-lengths, respectively, about the center, of the two ends of the principal axes if they are already horizontal and vertical or, if they are not, of the horizontal and vertical axes of the strong circle of reflections. The sense of each correction is determined by the fact that the longer end of a streak is directed out of the vertical plane *away from* the X-ray source.

(c) In setting photograph no.2 (Fig. 2b), the Y^* axis should be exactly horizontal, and the Y^* and Z^* streak lengths exactly symmetrical about the center of the film, indicating that the crystal is now rotating and precessing exactly about Y^* and X, respectively.

(d) The first of the two desired 0-level precession photographs, that around X, is now taken with the following changes in instrumental settings: Zr-

TABLE 3. MILLER INDICES hkl, QUALITATIVE INTENSITIES, LATTICE SPACINGS d(Å), AND PRECESSION PHOTO RECIPROCAL DISTANCES 2p*(mm) FOR PRINCIPAL REFLECTIONS ON X- AND Z-AXIS 0-LEVEL PRECESSION PHOTOGRAPHS OF MICROCLINE-ORTHOCLASE AND LOW ALBITE[1]

RECIPROCAL AXIS	RELEVANT (DIRECT) PRECESSION AXIS[2]	MICROCLINE-ORTHOCLASE				LOW ALBITE			
		hkl	Intensity[3]	d,Å[4]	2p*, mm[5]	Intensity[3]	d,Å[4]	2p*, mm[5]
x* = [100]*	z = [001]	200	VW	3.848	22.2	VW	3.639	23.4
		400	M	1.924	44.3	W	1.820	46.9
		600	VW	1.283	66.5	VW	1.213	70.3
y* = [010]*	X,Z,[203], [101],[102]	040	VS	3.243	26.3	VS	3.188	26.8
		060	S	2.162	39.4	W	2.125	40.1
		080	W	1.622	52.6	VW	1.594	53.5
		0.10.0	VW	1.297	65.8	VW	1.275	66.9
z* = [001]*	X = [100]	002	VS	3.240	26.3	VS	3.194	26.7
		003	VW	2.160	39.5	VW	2.129	40.1
		004	VW	1.620	52.6	VW	1.597	53.4
		005	VW	1.296	65.8	VW	1.278	66.7
$[\bar{4}03]^*$	[203]	$\bar{4}03$	W	1.910	44.7	M	1.849	46.1
$[\bar{1}01]^*$	[101]	$\bar{2}02$	VS	3.285	26.0	VS	3.214	26.5
		$\bar{4}04$	VW	1.643	51.9	VW	1.607	53.1
$[\bar{2}01]^*$	[102]	$\bar{2}01$	VS	4.215	20.2	VS	4.027	21.2
		$\bar{4}02$	S	2.107	40.5	VW	2.014	42.3
		$\bar{6}03$	VW	1.405	60.7	VW	1.342	63.5

[1] Applicable for MoKα radiation and crystal-to-film distance F=60.0 mm. See footnote 5. [2] For corresponding precession photographs, see Table 2. [3] V = very, S = strong, M = medium, W = weak. [4] From Borg & Smith 1969. Mean values for maximum microcline and orthoclase. [5] From one reflection to its equivalent through the film centre; p*(hkl) = λ x F/d(hkl) = 0.7107 x 60.0/d(hkl) mm. Slight differences between some of these 2p* values and corresponding values of a*, b*, c* in Table 4 are because of small differences in the source data in the two cases.

filtered Mo*K* radiation (Mo/Zr), *i.e.*, Mo*Kα* radiation; $\mu = 25°$; screen radius $r_s = 15$ mm, screen-to-crystal distance $s = 32.6$ mm. The resulting photograph for the desired orientation around *X* should resemble Figure 2c. Because of (1) the larger area of the reciprocal lattice recorded (larger μ), and (2) the better resolution of the individual reflections through the removal of most of the streaks (filter absorption of the white radiation), one should now be able to definitely identify the two principal axes by, if necessary, comparison with the standard 0-level photograph(s) or by means of Table 3.

The second desired photograph is the corresponding 0-level precession around *Z* that records the *X*Y** plane and the *hk*0 reflections.

(e) Because the angle between *X* and *Z* is β, the crystal need now only be rotated around *Y** by $\beta \approx 116°$ on the dial in order to orient *Z* along the X-ray beam (Fig. 3a). However, because one cannot know in this procedure whether the rotation should be clockwise or counterclockwise, one simply turns the crystal 116° in one direction and takes a 0-level photograph that will, if the sense is correct (Fig. 1b), resemble Figure 2e if the crystal is untwinned microcline. Because β is unlikely to be exactly 116°, the vertical streaks on this photograph can be used to give a (small) Δd correction, and the desired oriented photograph taken. (A *Z*-axis setting photograph, not normally necessary, is shown as Fig. 2d.) If in rotating the crystal through β the sense is wrong, the crystal will be precessing approximately around [203] (Figs. 1c, 3a), and the photograph will resemble that in Figure 4a.

In our experience, one may, with this procedure, fairly easily misorient or even misidentify the crystal in the first instance. Following are the most likely of these possibilities.

Misidentification. The only misidentification one is likely to make is to take albite for microcline or *vice versa*. If one is aware of this possibility, the standard photographs of microcline referred to above and of albite described below enable one to readily identify the crystal correctly.

Misorientation of microcline. Two such misorienta-

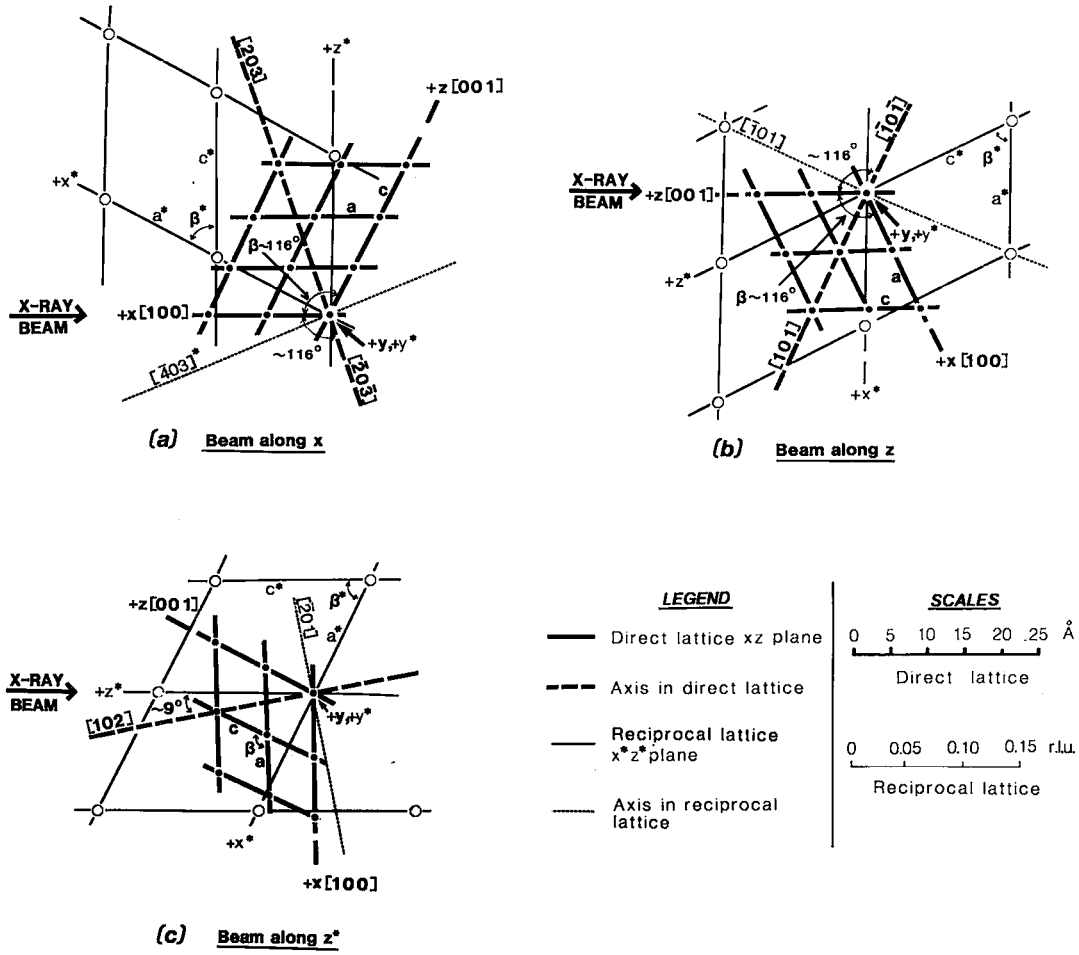

FIG. 3. Direct and reciprocal lattices of maximum microcline (Table 4) projected along Y, Y^* to illustrate the relationship of direct and reciprocal axes relevant to the procedure, especially the 'unintended' precession axes that may be obtained, as explained in the text and illustrated in Figure 4. Slight but negligible distortion of the lattices as shown arises from the fact that, because α and γ are 90.6° and 87.7°, respectively, rather than 90°, the direct and reciprocal lattices are not quite in the same plane. Scale of the reciprocal lattice units (r.l.u.) is arbitrarily chosen for convenient graphics. (a) A rotation of ~ 116° from X[100] giving $[20\bar{3}]$(= [203]) instead of Z[001] (Figs. 1a, c, 4a). (b) A rotation of ~ 116° from Z[001] giving $[\bar{1}0\bar{1}]$(= [101]) instead of X[100] (Figs. 1e, f, 4b). (c) Beam along normal to {001} cleavage = $Z^* \approx$ [102] instead of along X[100] (obtainable by a turn of ~ ± 90°) (Figs. 1d, a, 4c).

tions occurred sufficiently often during this study that they are worth noting.

(i) At step (a) in the *Orientation Procedure*, the crystal may be found to be inadvertently precessing about Z rather than X, possibly because of distinct development of a {100} 'Murchisonite' parting that could be mistaken for a {001} cleavage (Fig. 1e). As Figure 3b shows, a turn of $\beta = 116°$ in one sense will, of course, result in desired X being along the X-ray beam (Fig. la), whereas a turn in the other sense will, as a result of geometry, orient the undesired [101] direction along the beam (Figs. 1f, 3b) and give rise to a 0-level photograph (Fig. 4b) that superficially resembles the 0-level around X (Fig. 2c). The diamond-shaped pattern of the former easily differentiates it from the square pattern of the latter, but the user will find that, in general, care must be taken in identifying correctly all setting and 0-level photographs.

(ii) The second misorientation arises from the fact that, at the same step (a) in the preceding section, the 'wrong' rocker may be set parallel to the X-ray

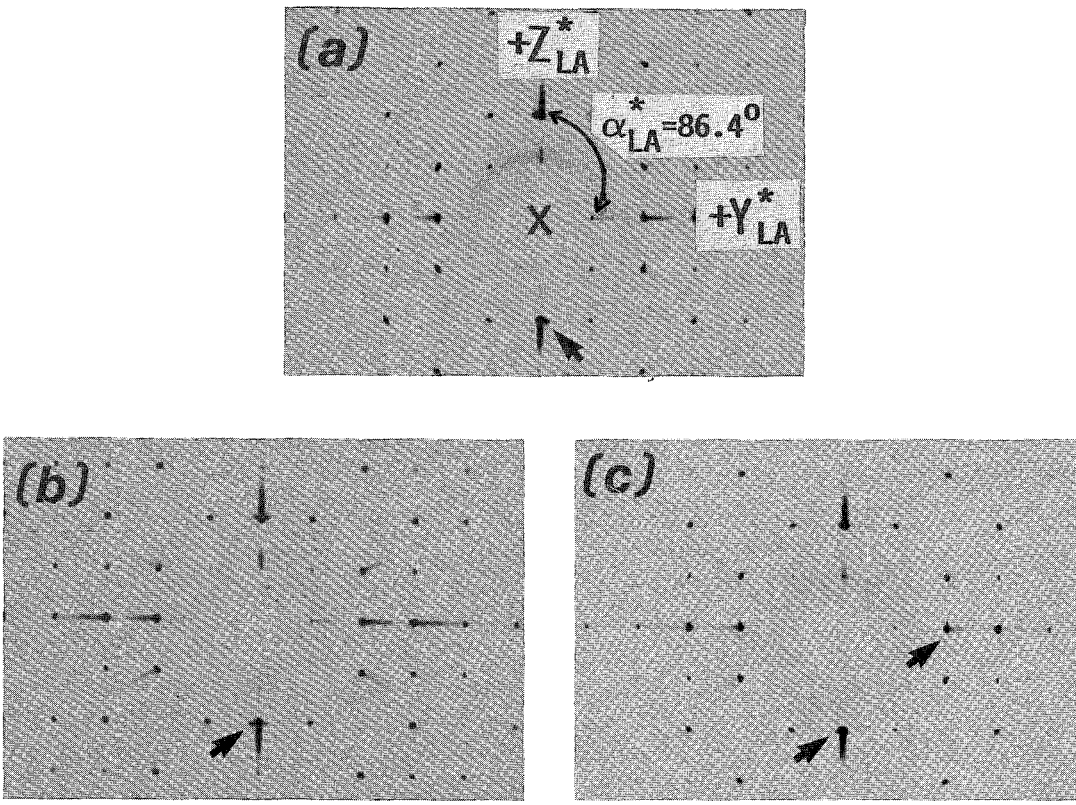

FIG. 4. 0-level precession photographs to scale of maximum microcline around 'unwanted' axes. See Figure 3 and text. Operating conditions as for the precession photographs in Figure 2. Precession axes, reciprocal planes and specimen identifiers as follows: (a) [203], Y^* [$\bar{4}$03]*, (MONO); (b) [$\bar{1}$01], Y^* [101]*, (PG–133); (c) [102], Y^* [$\bar{2}$01]*, (MLG–01).

beam because of small size of crystal or poor development of cleavage, resulting in the perpendicular to {001} = Z^* being oriented along the beam (Fig. 1d). The geometry is such (Fig. 3c) that the [$\bar{1}$02] direction is then the precession axis, and the 0-level photograph will be like that shown as Figure 4c. When this is recognized, the crystal is then rotated + 90° in order to orient X along the X-ray beam.

Interpretation of Albite and Pericline Twinning of Microcline from Precession Photographs

Available to the investigator at this stage are the two 0-level precession photographs, one precessing about X and the other about Z, recording the Y^*Z^* and X^*Y^* reciprocal planes and the $0kl$ and $hk0$ reflections, respectively. The interpretation of these photographs falls into four different categories, which correspond to the four kinds of information that can be derived from them (listed in the Introduction). Although interrelated in some cases, it is appropriate to first describe each kind of feature separately.

The reciprocal-lattice geometry and the indexing of reflections of X- and Z-axis 0-level precession photographs of untwinned and twinned K-feldspar

It is essential to the interpretation of the photographs, which are undistorted records of the reciprocal lattice, that one be familiar with the relevant lattice-geometry and the indexing of the reflections of both untwinned and twinned K-feldspar. Figures 5a–g are diagrammatic representations drawn to the same scale (except for Fig. 5g) as the photographs of the 0-level reciprocal-lattice planes Y^*Z^* and X^*Y^* most likely to be found in untwinned and twinned crystals of K-feldspar [*cf.* Figs. 6.1 and 6.2 in Smith & Brown (1988) or in Smith (1974)].

The reciprocal lattice parameters a^*, b^*, c^*, α^*, β^*, γ^* that characterize these two reciprocal lattice planes are related to the direct-cell parameters a, b, c, α, β, γ by mathematical formulae given in such

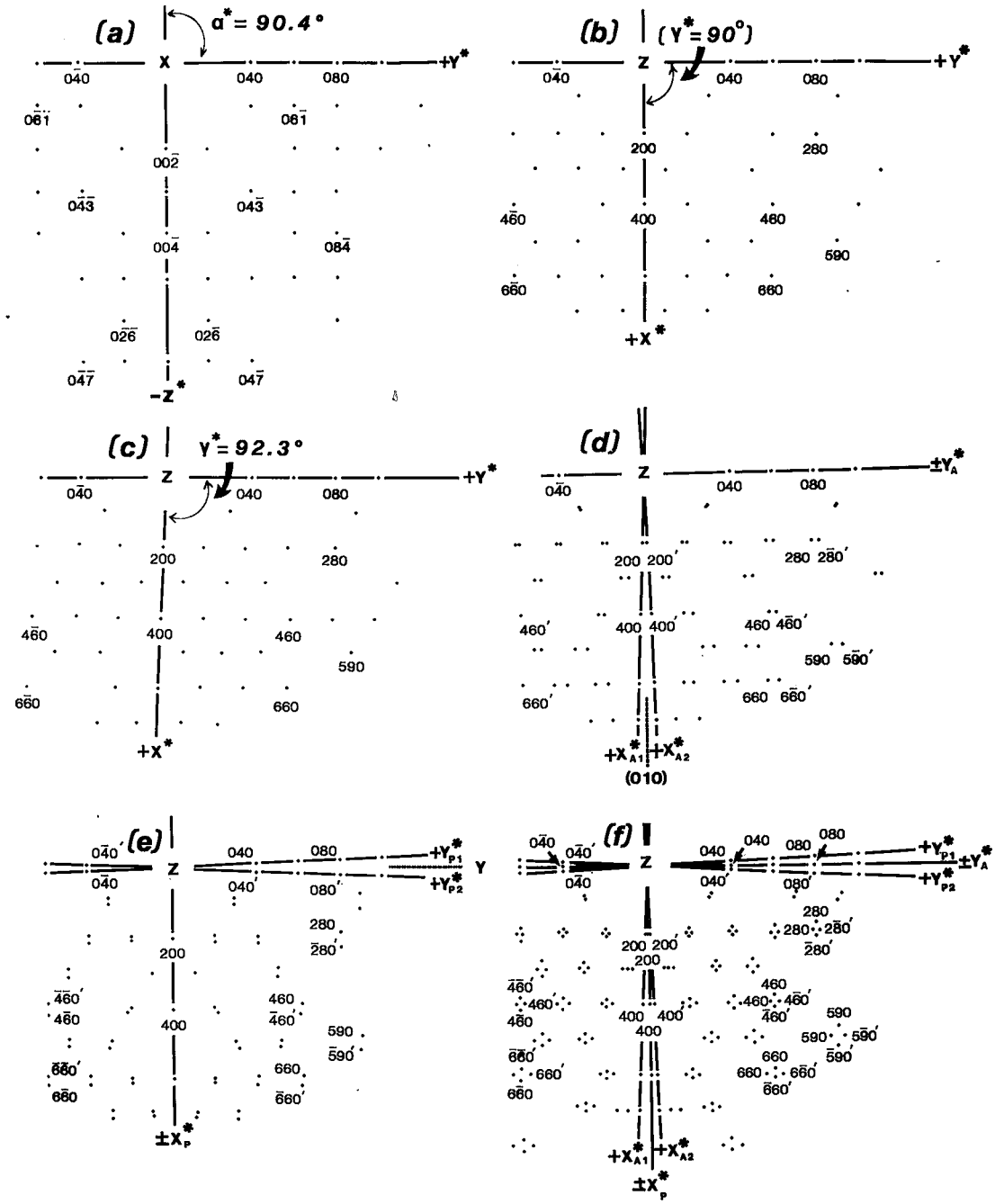

FIG. 5. Diagrammatic representation of the reciprocal lattice planes Y^*Z^* and X^*Y^* of maximum microcline and orthoclase corresponding to the 0-level precession photographs in Figure 6, showing the labeling of the axes and the indexing of some reflections. Figures a–f are on the same scale as the photographs in Figure 6, and in these diagrams, unprimed indices are for individuals A1, P1, primed for A2, P2. In g the scale is enlarged for clarity. (For similar diagrams see, *e.g.*, Smith & Brown 1988, Figs. 6–1 and 6–2, and McLaren 1984, Fig. 1). The direct axis normal to each reciprocal plane (X in a, Z in all others) is the precession axis in the corresponding photographs in Figure 6. (a) Maximum microcline, untwinned, X axis, Y^*Z^* plane, reflections $0kl$; the corresponding lattice plane of albite- or pericline-twinned microcline and of orthoclase would be virtually identical to this (Fig. 6a); (b) orthoclase, 'untwinned', Z axis, X^*Y^* plane, $hk0$ reflections (Fig. 6b); (c)–(g) maximum microcline, Z axis, X^*Y^* plane, reflections $hk0$; (c) untwinned (Fig. 6c); (d) albite-twinned (Fig. 6d); (e) pericline-twinned (Fig. 6e); (f), (g) M-twinned (Fig. 6f) with scale expanded and γ^* exaggerated in g for clarification of axis labels and indices of lattice points.

texts as Nuffield (1966). Table 4 gives the space-group symmetry and the direct and reciprocal unit-cell parameters of maximum (low) microcline, orthoclase and low albite.

In this procedure, the orientation of the crystals is such that Y^* is horizontal and X^* and Z^* quasi-vertical in the Z- and X-axis projections, respectively. In twinned crystals, certain of the axes are doubled

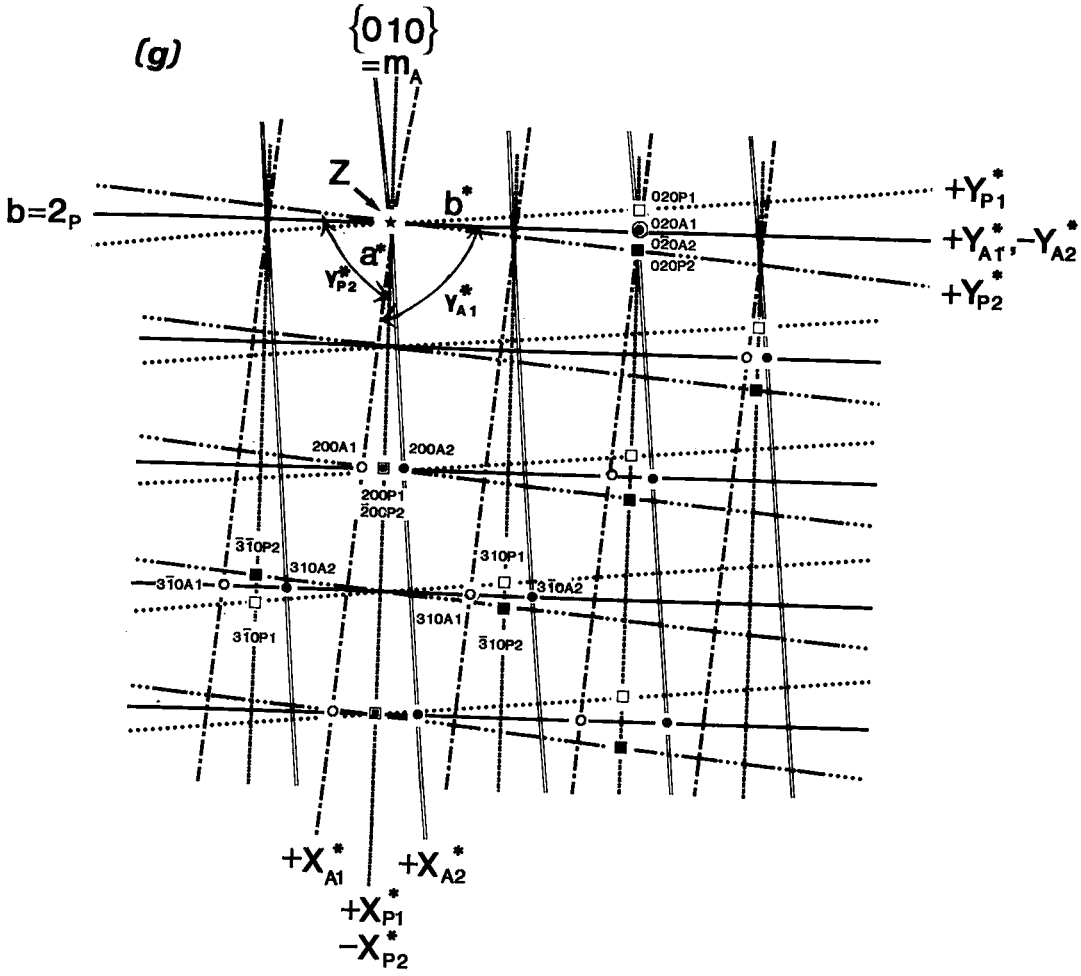

LEGEND (g)

Unit	Indexing	Reflection	Lattice
albite–twin 1	hk0A1	o	
albite–twin 2	hk0A2	•	
pericline–twin 1	hk0P1	□	
pericline–twin 2	hk0P2	■	
overlapped A1, A2 rows			
overlapped P1, P2 rows			

TABLE 4. DIRECT AND RECIPROCAL UNIT-CELL PARAMETERS OF RELEVANT ALKALI FELDSPARS

Feldspar	Ideal Formula	System Space Group	a,Å a*, nm[1]	b,Å b*, nm[1]	c,Å c*, nm[1]	α α*	β β*	γ γ*	V,Å³ V*x10²,Å⁻³	source[2]
maximum (low) microcline	$KAlSi_3O_8$	triclinic $C\bar{1}$	8.592 5.524	12.963 3.293	7.222 6.567	90.62° 90.44°	115.95° 64.05°	87.67° 92.29°	722.6 0.1384	a
'orthoclase' (monoclinic K-feldspar)	$KAlSi_3O_8$	monoclinic C2/m	8.601 5.518	12.995 3.281	7.202 6.590	-- --	116.04° 63.96°	-- --	723.2 0.1383	b
low albite	$NaAlSi_3O_8$	triclinic $C\bar{1}$	8.135 5.862	12.785 3.345	7.158 6.676	94.27° 86.39°	116.60° 63.49°	87.68° 90.46°	663.8 0.1506	a

[1] Reciprocal periods a*, b*, c* scaled as in Table 3, footnotes 1 and 5 in order to be directly applicable to the precession photos in this paper and to the 2p* values in Table 3. [2] (a) Kroll & Ribbe (1987, Table 4); (b) Hovis (1986, Table 6,) for his Or-richest orthoclase 7738, Or_{96}.

TABLE 5. SUMMARY OF INFORMATION DERIVED FOR THE MICROCLINE, ORTHOCLASE AND ALBITE SPECIMENS BY THE PRECESSION AND POWDER PROCEDURES[1]

specimen number	precession						powder				
							Gandolfi[2]		diffractogram[3]		
	phase(s)[4]	estim. wt. %	twin type[5]	γ*(microcl.) α*(albite)	tricl. Δ[6] (K-feldsp.)	streak type[7]	estim. wt. %	tricl. Δ[8] (K-feldsp.)	estim. wt. %[9]	tricl. Δ[8] (K-feldsp.)	γ*(microcl.) α*(albite)[10]
AEC-20	MM	99	U	92.5(2)°	1.08(9)	un	99	1.05(5)	>95	0.95(2)	92.3(1)°
	LA	1	U	86.3(1)°	--	un	1	--	<5	--	--
APG-05	MM	99½	M	92.4(1)°	1.04(4)	un	100	0.99(5)	75	0.97(2)	92.3(1)°
	LA	½	A	86.5(2)°	--	un	--	--	25	--	--
CG-03	MM	98	A	92.3(1)°	1.00(4)	A1↔A2	98	0.96(5)	75	0.93(2)	92.2(1)°
	LA	2	A	86.5(1)°	--	un	2	--	25	--	--
CG-03AB	LA	100	U	86.3(1)°	--	un	100	--	100	--	86.22(5)°
GPE-11	MM	99½	M	92.2(1)°	0.95(4)	A1↔P1 A2↔P2	99½	1.05(5)	80	0.91(2)	92.2(1)°
	LA	½	A	86.5(2)°	--	un	½	--	20	--	--
MLG-01	MM	99½	U	92.4(1)°	1.00(4)	un	100	1.00(5)	95	0.96(2)	92.2(1)°
	LA	½	U	86.3(1)	--	un	0	--	5	--	--
MLP/NZ-24	MM	5	A	92.0(2)°	0.87(8)	A1↔OR↔A2	70	0.73(5)	65	0.63(2)[11]	91.4(3)°[11]
	IM(=OR)	95	U	90.5(1)°	0.22(1)		29½	0	>35		
	LA	½	A	86.3(1)°	--	un	½	--	<5		--
MONO	OR	100	-	90.0(1)°	0	un	100	0	100	0	90.0(1)°
PG-24	MM	99½	M	92.2(1)°	0.96(4)	un	100	1.01(5)	>95	1.03(2)	92.35(3)°
	LA	½	A	86.4(1)°	--	un	0	--	<5	--	--
PG-121	MM	100	U	92.4(2)°	1.05(8)	un	100	1.05(5)	95(LA 5)	1.01(2)	92.38(7)°
PG-133	MM	99½	A	92.2(2)°	0.98(9)	un	100	1.00(5)	>95	1.02(2)	92.38(7)°
	LA	½	A	86.4(2)°	--	un	0	--	<5	--	--
PG-138AB	K-f	3	-	--	--	un	2	--	2	--	--
	LA	97	A	86.6(2)°	--	un	98	--	98	--	86.47(7)°
SR-97	MM	98	M	92.3(1)°	1.00(4)	A1↔(P1) A2↔(P2)	98	1.00(5)	85	0.99(2)	92.4(1)°
	LA	2	M	86.3(2)°	--	un	2	--	15	--	--
SR-148	MM	99½	P	92.2(1)°	0.98(4)	(A1)↔P1 (A2)↔P2	100	1.00(5)	85	0.99(2)	92.38(3)°
	LA	½	A	86.4(1)°	--	--	0	--	15	--	--

[1] Note: (a) For source and compositions, see Table 1. (b) Data mainly from McGregor 1984, Table 3-2 but see other footnotes. [2] Modified from McGregor 1984, Table 3-6 for the precession crystal. [3] From McGregor 1984, Table 3-9 for a bulk sample. [4] MM=maximum microcline, IM=intermediate microcline, OR=orthoclase, K-f=K-feldspar, LA=low albite. [5] U=untwinned, A=albite-twinned, P=pericline-twinned, M=M-twinned. [6] $\Delta=(\gamma^*-90^\circ)/2.29^\circ$ (see text). [7] un=unstreaked; for the meaning of A1<->P1, etc., see text. [8] $\Delta=12.5[d(131)-d(131)]$. [9] The much higher amount of albite than from the single-crystal precession and Gandolfi records is due to the fact that the sample is bulk. [10] From refined unit cell parameters (McGregor 1984, Table 3-7). [11] For the K-feldspar mixture.

(or tripled) as noted below. Interaxial angles α^* and γ^* are contained by the + Y^*,+ Z^* and the + X^*, + Y^* axes, respectively. The periods a^*, b^*, c^* are shown along X^*, Y^*, Z^*, respectively, but with the following qualifications.

Regarding the indexing of the reflections, in general the h, k, l indices of a reflection are simply its a^*, b^*, c^* coordinates along X^*, Y^*, Z^* from the center of the film (the origin); Figure 5 shows the indices of some representative reflections. However, microcline, orthoclase and low albite all have space-group symmetry based on a C lattice (Table 4), and this results in the systematic absence of hkl reflections with $h + k \neq 2n$. Thus in all the lattices, only the $0k0$ Y^*-reflections 020, 040, *etc.*, separated by $2b^*$ will, in general, appear (although random absences among systematically present reflections are possible); similarly, only the $h00$ X^*-axis reflections 200, 400, *etc.*, separated by $2a^*$ will, in general, appear. However, the $00l$ Z^*-axis reflections are unaffected by the C-lattice condition, and in general will appear 'in all orders', *i.e.*, 001, 002, *etc.*, separated by c^*.

Note that in Figures 5a–g, only one-half of each reciprocal lattice plane is shown. Because of the center of symmetry introduced into the center of all 0-level precession photographs by the X rays

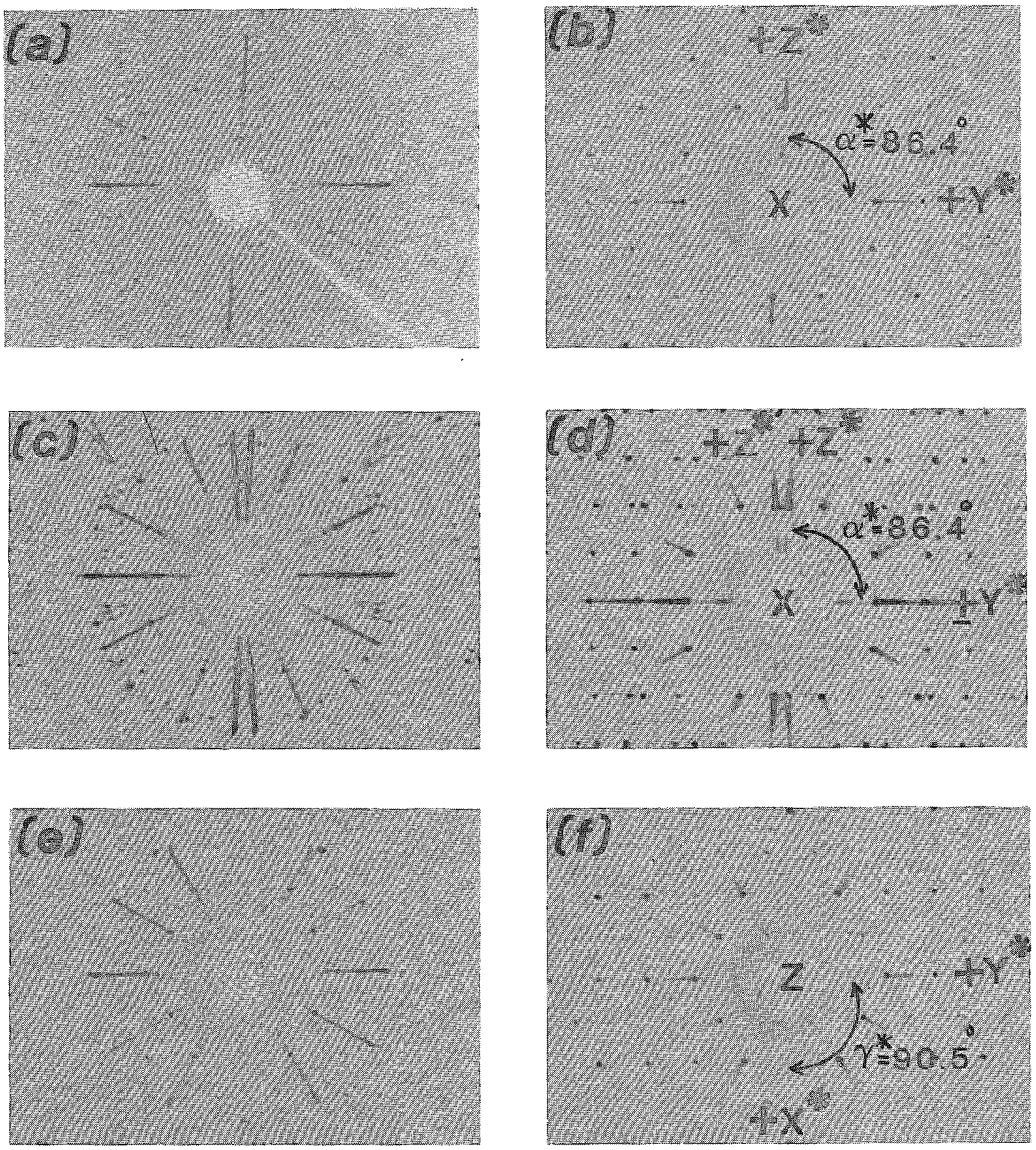

FIG. 6. Diagnostic 0-level precession photographs to scale of maximum microcline and orthoclase. For the labeling of the axes in d, e, f and for the indices of the reflections in all photographs, see Figures 5a–g. Radiation Zr-filtered Mo$K\alpha$, $\mu = 25°$; other experimental conditions as for the 0-level precession photographs in Figures 2c, e. (a) Maximum microcline, albite-twinned, *X* axis (PG–24). Because of the closeness of α^* to 90°, the comparable photographs of untwinned and pericline- or *M*-twinned maximum microcline and of orthoclase are nearly identical to this one. Albite-twinned $00\bar{2}$ reflections of (perthitic) low albite flank the $00\bar{2}$ reflection of the microcline. (b) Orthoclase, *Z* axis (MONO). (c) Maximum microcline, untwinned, *Z* axis (PG–121). The γ^* angle shown is the 'ideal' (Table 4) rather than the specific values (Table 5). (d) Maximum microcline, albite-twinned, *Z* axis (PG–24). (e) Maximum microcline, pericline-twinned, *Z* axis (SR–148). (f) Maximum microcline, *M*-twinned, *Z* axis (APG–05).

('Friedel's law'; see, for example, Nuffield 1966, p. 86), the half of the lattice plane shown in all but Figure 5b is representative of the whole plane recorded on a precession photograph; Figure 5b is, as explained below, representative of two units of the plane.

Twinning of microcline and characteristics of orthoclase

In what follows, the reader will find it convenient to refer to Tables 1, 2, and 5 in addition to the Tables and Figures specified.

X-axis precession. (Figs. 5a, 6a). The Figures represent, in effect, the Y^*Z^* plane of an untwinned K-feldspar. Because in maximum microcline $\alpha^* \approx 90.44°$ (Table 4), the small departure from 90° of ~ 1/2° makes the measurement of α^* imprecise and its diagnostic usefulness limited. This small departure also results in the fact that in albite- or pericline-twinned microcline, the separation in each of the Z^* and Y^* axes is almost imperceptible (Fig. 6a). Thus X-axis reciprocal-lattice projections and precession photographs of albite- and pericline-twinned microcline differ little from their untwinned counterparts and, indeed, from those of orthoclase ($\alpha^* = 90°$). Therefore Figures 5a and 6a may be taken to represent all of untwinned and albite- and pericline-twinned microcline, and orthoclase.

Orthoclase ('untwinned'), Z-axis precession. (Figs. 5b, 6b). The 90° angle ('γ^*') between + X^* and + Y^* and the equal intensities of many reflection pairs will reveal {010} as a mirror plane perpendicular to Y, and Y (= Y^*) as a 2-fold axis. The crystal thus is monoclinic $2/m$, and albite and pericline twinning are impossible. The angle γ^* should, however, be measured carefully because if γ^* exceeds 90.1°, the crystal is, within the limit of measurement error of 0.1°, triclinic and hence a low-Δ microcline (see *Triclinicity*, below).

For monoclinic $C2/m$ crystals like orthoclase, one quadrant of a principal reciprocal-lattice plane (*i.e.*, one-half of Fig. 5b and one-quarter of Fig. 6b) constitutes a representative unit because mirror plane {010} equates reflection pairs $hk0$, $\bar{h}k0$, and the 2-fold axis equates pairs $hk0$, $\bar{h}k0$ (Fig. 5b).

Untwinned maximum microcline, Z-axis precession. (Figs. 5c, 6c). The angle $\gamma^* \sim 92.3°$ (Table 4) and the absence of doubling of the X^*- and Y^*-axis reflections reveal the untwinned character of the crystal. (For an intermediate microcline, $90° < \gamma^* < 92.3°$; see below under *Triclinicity*.) Because the space group $C\bar{1}$ has only a center of symmetry, the only equivalence of reflections is, as explained above, through the origin, *i.e.*, $hk0 = \bar{h}\bar{k}0$, and one-half of a principal lattice-plane, *i.e.*, the whole of Figure 5c and one-half of Figure 6c, constitutes a representative unit. The same situation holds for all other projections and photographs of microcline shown in Figures 5 and 6 (as well as those shown later for albite).

Albite-twinned maximum microcline, Z-axis precession. (Figs. 5d, 6d). The albite twin-law, reflection in {010}, results in the coincidence of the twinned pairs of reflections $0k0_{A1}$ and $0k0_{A2}$ along the + Y_{A1}^* and $-Y_{A2}^*$ (and opposite) axes, but all other reflections are doubled. In particular, with $\gamma^* \approx 92.3°$ and $\gamma^* - 90° \approx 2.3°$, the axes + X_{A1}^* and + X_{A2}^* defined by the reflections $h00_{A1}$ and $h00_{A2}$ diverge and subtend an angle of ~ 4.6°. (For an intermediate microcline, this angle would be less than 4.6° but greater than 0.) The trace of the twin plane {010} ideally bisects this angle. A measurement of this angle provides a convenient, precise way of determining γ^*.

Pericline-twinned maximum microcline, Z-axis precession. (Figs. 5e, 6e). The pericline twin-law, which involves a 180° rotation about the Y axis, results in the coincidence of the twinned pairs of reflections $h00_{P1}$ and $\bar{h}00_{P2}$ along the + X_{P1}^* and $-X_{P2}^*$ (and opposite) axes, but all other reflections are doubled. In particular in this case, the + Y_{P1}^* and the + Y_{P2}^* axes diverge and subtend the angle of ~ 4.6° (or less for an intermediate microcline). The twin axis Y ideally bisects this angle.

Albite- and pericline- (M-) twinned maximum microcline, Z-axis precession. (Figs. 5f,g, 6f). The reciprocal-lattice pattern and precession photograph can be regarded as composites of their individually twinned counterparts (Figs. 5d,e, 6d,e) described above. Principal axial reflections occur as triplets made up of a pair of outside reflections related by one twin law, and a central reflection consisting of the superimposed pair of reflections related by the other law. For example, along + X^*, outer pair 400 and 400′ are related by the albite law (and are thus 400_{A1} and 400_{A2}), and the reflection between them consists of the superimposed pericline-law-related pair 400_{P1} and $\bar{4}00_{P2}$. In contrast, nonaxial reflections consist of quadruplets in rhombic or distorted rhombic configurations (depending upon their location on the film), in which horizontal pairs are related by the albite law, vertical pairs by the pericline law (Fig. 5g).

Standard Precession-Photographs of Untwinned and Albite-Twinned Low Albite

Standard precession-photographs of low albite can serve two purposes: (i) to examine a single crystal of an albite specimen in order to derive essentially the same kinds of information obtainable for a microcline crystal; and (ii) to provide an interpretation of the geometry and twinning of the albite commonly revealed by single-crystal and powder X-ray records of microcline to occur as a second phase (in our case, in 27 out of 29 specimens). Figures 7a–f reproduce standard setting and 0-level precession photographs of two specimens of low albite whose origins and relevant crystal-chemical characteristics are given in Tables 1 and 5 (see also Tables 2–4).

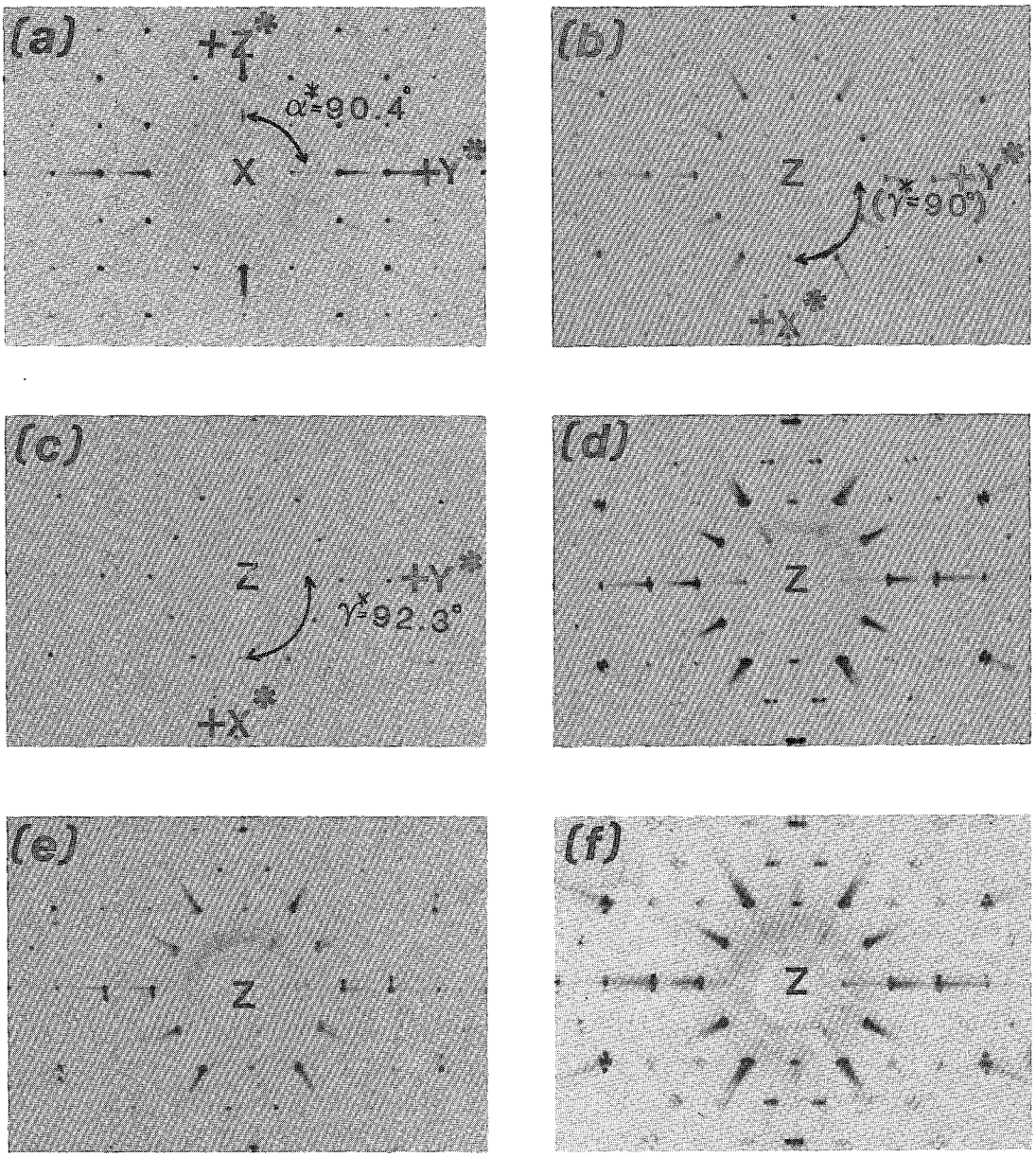

FIG. 7. Diagnostic setting and 0-level precession photographs to scale of low albite comparable to most of those for maximum microcline in Figures 2 and 6. Experimental conditions as for those in Figure 2. The α^* and γ^* angles shown are the 'ideal' (Table 4) rather than the specific values (Table 5). (a), (b) Untwinned, setting and 0-level, respectively, *X* axis (both CG-03AB) (*cf.* Figs. 2b, c, 6a, especially the different α^* values). (c), (d) Albite-twinned, setting and 0-level, respectively, *X* axis (both PG-138AB). (e), (f) Albite-twinned, setting and 0-level, respectively, *Z* axis (both CG-03AB) (*cf.* Figs. 2d, e, 6c, d, especially the different γ^* values).

The following points may be made about the precession photographs of low albite.

(a) Three of the reciprocal-lattice parameters in albite, a^*, α^*, γ^*, differ sufficiently from their counterparts in microcline (Table 4) that corresponding precession photographs may readily be differentiated: in low albite, a^* is larger, and the departures from 90° of α^* and γ^* are larger and smaller,

respectively, than in microcline. These differences can be seen easily in the comparable photographs shown as Figures 6a and 7b, and 6c and 7f.

(b) The differences in the unit cells of the two minerals, especially in a^*, are sufficiently large that comparable X-axis *setting* photographs can be easily distinguished (Figs. 2a,b and 7a). The identification of the alkali feldspar crystal should thus be clear from the outset.

(c) Because albite and, to a first approximation, all Na-rich plagioclases have, like microcline, a triclinic C lattice, one representative unit consists of one-half a reciprocal lattice-plane. The four quadrants in Figures 7b, d, f thus make up two representative units.

(d) Despite the unit-cell differences between albite and microcline noted under (a), comparable lattice planes are sufficiently similar that the indexing of the reflections shown for microcline in Figure 5 can be applied to the albite photographs shown as Figures 7b, d and f.

(e) No pericline-twinned albite is included in Figure 7 because none was observed in our two albite specimens (Table 1) or in the albite intergrown in 27 out of 29 of our microcline specimens.

Triclinicity, Relative Amounts of Twin Components, and Nature of Multiphase Crystals of Microcline and Orthoclase from Precession Photographs

Triclinicity

The 'triclinicity' (Δ) of a K-feldspar (Goldsmith & Laves 1954) has been widely used to rank a K-feldspar between the structural extremes maximum microcline and monoclinic K-feldspar. Other 'triclinic indicators' are possible (see, *e.g.*, Smith 1974, p. 285-289) including γ^*, whose departure from 90° may vary from 2.29° (Table 4) ($\Delta = 1$) to 0° ($\Delta = 0$). (Because the maximum difference from 90° of angle α^* is only ~ 0.44° (Table 4), values derived from this angle are too inaccurate to be of use.) Angle γ^* may easily be read from Z-axis precession photographs of untwinned (Fig. 6c) or twinned (Figs. 6d–f) microcline as the angle between the $+ X^*$ and $+ Z^*$ axes. Assuming $\gamma^* = 92.29°$ for maximum microcline (Table 4), then

$$\text{triclinicity } \Delta = \frac{\text{measured } \gamma^* - 90°}{2.29°}.$$

For a measurement error in γ^* of 0.1°, the error in Δ is ~ 5 in 100.

In this paper, the relevant K-feldspar phases are defined on the assumption of a γ^* error of 0.1° as follows: *maximum microcline* $\Delta > 0.85$, $\gamma^* > 92.0°$; *intermediate microcline* $0.05 < \Delta < 0.85$, $90.1° < \gamma^* < 92.0°$; *orthoclase* [(metrically) monoclinic K-feldspar] $\Delta = 0 \pm 0.05$, $\gamma^* = 90.0 \pm 0.1°$. Table 5 gives the γ^* values and the triclinicities derived from them for all the K-feldspar specimens referred to in this paper, including the two that follow, which we cite as examples.

Example 1. Untwinned microcline PG–121 (Fig. 6c). $\gamma^* = + X^* \wedge + Y^* = 92.4(2)°$ (Table 5), $\Delta = [92.4(2)-90]/2.29 = 1.05(8)$, *i.e.*, maximum microcline.

Example 2. Albite-twinned microcline PG–24 (Fig. 6d). $\gamma^* = + X^* \wedge + Y^* = 92.2(1)°$ (Table 5), $\Delta = [92.2(1)-90]/2.29 = 0.96(4)$, *i.e.*, maximum microcline.

Evaluation of relative amounts of twin components

In principle, it should be possible to evaluate the relative volumes of the different components of a twin from the relative intensities on precession photographs of the twin-related reflections. However, Smith (1974, p.185) has pointed out some of the problems in doing this, particularly for M-twinned microcline crystals, which relate to the planarity in reciprocal space of the reciprocal-lattice points whose reflections on the precession photographs are used for the intensity measurements. Nevertheless, under certain conditions, some reasonable evaluation of the relative volumes may be made, and we give two examples below. Two conditions should be met: (i) the reflections used should be from twin-related lattice planes that are structurally equivalent or nearly so, and (ii) the reflections should be weak enough (grey rather than black) that the intensity can be measured or estimated as a function of the darkening. In the following two examples the reflections come close to fulfilling these conditions. Intensities were simply estimated visually, and the results can be regarded as only semiquantitative.

Example 1. Albite-twinned microcline, specimen PG–24 (Fig. 6d; see also Figs. 5d, g.) The rotation axis is Y^* common to both twinned individuals, and the two X^*Y^* planes are coplanar with the film, so that no differences in intensity arise from precession geometry. Reflections along and close to the two X^* axes are from equivalent or quasi-equivalent lattice planes. From reflection pairs 620_{A1}, $\bar{6}\bar{2}0_{A2}$, and $6\bar{2}0_{A1}$, 620_{A2} and their $\bar{h}$ equivalents, the intensity I ratio $I(A1):I(A2)$ is approximately equal to 3:1, from which the estimated volumes of A1 and A2 are inferred to be approximately 75% and 25%, respectively.

Example 2. M-twinned microcline, specimen APG–05. (Fig. 6f; see also Figs. 5f, g.) Although, as noted above, all reciprocal-lattice points in this case are not strictly coplanar, they are, in our opinion, sufficiently close to being so that an approximate evaluation of the relative amounts of the four

twin components can be made using equivalent or quasi-equivalent reflections along or close to the + X^* and the + Y^* axes. Nonaxial quadruplets may be used, but one must be cautious about the nonequivalence of the reflections (Fig. 5g). From the following reflections (observable only on the original photographs) $7\bar{1}0_{A1}$, $7\bar{1}0_{A2}$ and their $-h$ and $-k$ equivalents; $7\bar{1}0_{P1}$, $7\bar{1}0_{P2}$ and their $-h$ and $-k$ equivalents; and $0.10.0_{A1,A2}$, $0.10.0_{P1}$, $0.10.0_{P2}$ and their $-k$ equivalents, were derived the relative intensities I(A1):I(A2):I(P1):I(P2) ≈ 8:24:10:1, from which the estimated volumes are inferred to be A1 ≈ 19%, A2 ≈ 56%, P1 ≈ 23%, P2 ≈ 2%, from which (A1 + A2) ≈ 75%, (P1 + P2) ≈ 25%.

Nature of multiphase K-feldspar crystals

Some K-feldspar crystals, including those of 'precession size', are found by X-ray diffraction to consist of two or more microcline phases of different triclinicity, and possibly also a monoclinic phase. Although multiphase character may be apparent in data obtained from powder records, precession photographs normally differentiate the phases more satisfactorily because equivalent reflections do not overlap.

Example. K-feldspar no. MLP/NZ 24 (Fig. 9b below, neglecting the streaks). General: albite-twinned microcline (phases M_{A1}, M_{A2}) plus (quasi-) monoclinic 'orthoclase' (phase O) (with some albite as described below). Details (Table 5): $\gamma^*(M_{A1}) = \gamma^*(M_{A2}) = 92.0(2)°$, $\Delta = 0.87(8)$; $\gamma^*(O) = 90.5(1)°$, $\Delta = 0.22(1)$. Relative volumes of the phases from the estimated intensities I of the triplet reflections along and near + X^*: $I(M_{A1}):I(M_{A2}):I(O) = 10:1:190$; $M_{A1} \approx 5\%$, $M_{A2} \approx 1/2\%$, $O \approx 95\%$. Conclusion: (low-Δ) intermediate microcline (close to orthoclase) approx. 95%, plus albite-twinned maximum microcline approx. 5% + 1/2%.

Sharp *versus* Streaked Reflections and their Interpretation

X-ray powder records of alkali feldspar have, typically, sharply defined peaks. For some samples, however, some peaks may be broadened as a result of transitional or coherent rather than sharp or incoherent boundaries between structural units or domains, *i.e.*, between twin components or different phases. The broadened peaks of powder records appear on precession photographs as streaks between adjacent reflections. Because each reflection is unique, single-crystal photographs provide a more powerful tool for interpretations than a powder record. Interpretations of streaked reflections on alkali feldspar photographs have been treated by Laves (1950, 1952), Laves & Goldsmith (1961), Laves & Soldatos (1962, 1963), and Soldatos (1962). A valuable summary is given by Smith (1974, p. 181-197).

Presented below are a systematic description and a simple designation of the different types of sharp and streaked reflections observed in our precession photographs (Figs. 6, 9), and a proposed interpretation of these and related types of reflections in terms of schematic 2-dimensional diagrams of the (direct) lattice (Figs. 8, 10). These diagrams are of the type used by Laves (1950, Figs. 4, 8) and Marfunin (1966, Fig. 27). Electron microscopy and diffraction of the last decade or so have shown that, for some types of streaked reflections, the actual situation is more complex than that suggested by the schematic diagrams of the previous and present authors. However, because several types of streaked reflection have yet to be explained by electron microscopy and diffraction, we feel that the diagrams shown in Figures 8 and 10 serve a purpose by providing one with a visual interpretation, albeit oversimplified, of the reflections and streaks observed on precession photographs.

Sharp pairs of albite- or pericline-twinned microcline reflections: two incoherent components (A1–A2 or P1–P2) (Figs. 6d,e, 8a,b). The cells in Figures 8a and b are oriented to conform to succeeding diagrams. Figure 6e of the pericline-twinned crystal is the closest in our suite to this type.

Triplets consisting of albite- or pericline-twinned microcline plus orthoclase reflections: one pair of microcline twin components separated through incoherent boundaries by an orthoclase domain (A1–O–A2 or P1–O–P2) (Figs. 8c and d). The reflections of orthoclase appear half-way between the pairs of those for the albite- or pericline-twinned components. Our suite of specimens does not include this type.

Quadruplets of sharp reflections in M-twinned microcline: two pairs of microcline components separated by incoherent boundaries (A1–A2 plus P1–P2) (Figs. 6f and 8e). The schematic lattice (Fig. 8e) may be compared with the model of Marfunin (1966, Fig. 27, left). An actual example examined by electron microscopy and diffraction was shown by Fitz Gerald & McLaren (1982) to consist of domains of albite twins completely enclosed in a matrix of pericline twins (but see further below under streaked reflections).

Quintuplets of sharp M-twinned microcline plus orthoclase reflections: pairs of albite- and pericline-twinned microcline components with at least one twin pair separated by incoherent boundaries from orthoclase domains (A1–O–A2 plus P1–O–P2, or A1–O–A2 plus P1–P2, or A1–A2 plus P1–O–P2) (Fig. 8f, A1–O–A2 plus P1–P2). This figure may be compared with Figure 8A of Laves (1950). None of our specimens gave this pattern of reflections, but

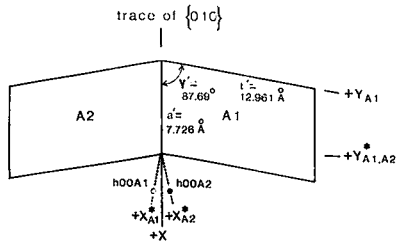

(a) Albite-twin.

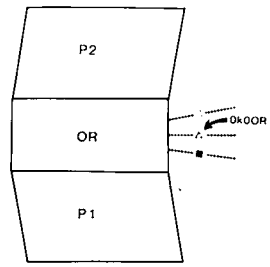

(d) Pericline-twin+orthoclase.

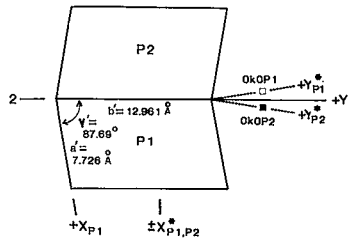

(b) Pericline-twin.

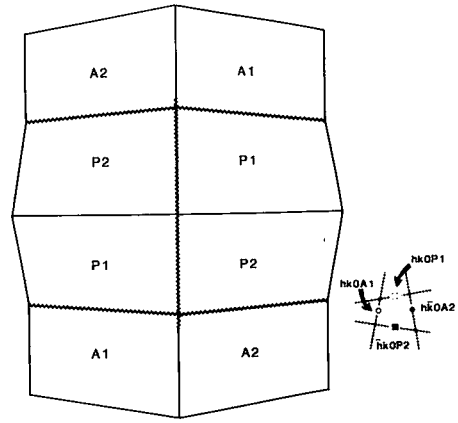

(e) M-twinned.

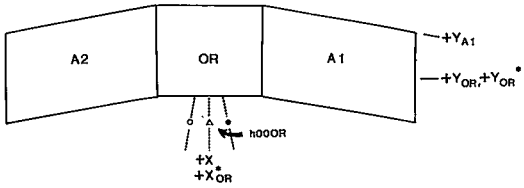

(c) Albite-twin + orthoclase.

LEGEND

(Figures 8 and 10)

unit cells	
direct cell outline	——
reciprocal cell axis	·····
domain designations	
albite-twins 1,2 of microcline	A1,A2
pericline-twins 1,2 of microcline	P1,P2
"orthoclase" (=monoclinic phase)	OR
reciprocal lattice points/reflections	
A1,A2	○ ●
P1,P2	□ ■
OR	△
interdomain boundaries	
contiguous and sharp	——
impossible or uncertain	~~~~
transitional	⟺
reflection streaks	
graphical (e.g.)	○—●
designation (e.g.)	A1 ⟷ A2

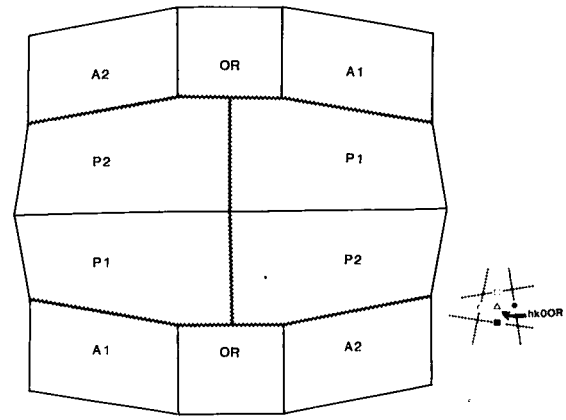

(f) M-twinned+orthoclase.

FIG. 8. Simplified diagrammatic 2-dimensional models of the direct lattices of maximum microcline and orthoclase

Figure 4 of Laves & Soldatos (1963) could be taken to represent it if one assumes an absence of inter-reflection streaks.

Streaked pairs of albite- or pericline-twin-related reflections in microcline: a pair of microcline twin components separated by coherent boundaries (A1↔A2 or P1↔P2) (Figs. 9a and 10a,b). The transitional zones will be twinned intermediate microcline with possible gradation through fine orthoclase, in which case this type is gradational to the one following. The streaks between the twin-related *Y**-axis reflections on the pericline-twin photograph in Figure 6e approach this type.

Streaked albite- or pericline-twinned microcline plus orthoclase reflections; a pair of microcline twin components and an orthoclase domain separated by coherent boundaries (A1↔O↔A2 or P1↔O↔P2) (Figs. 9b, 10c,d). This type is transitional with respect to the preceding. The pericline-twinned version of this has never been encountered. Four possible different lattice-models for albite-twinned versions are shown in Figure 10c. If pericline-twinned versions exist, comparable lattice-models could be drawn.

Streaks through each reflection of an albite- or pericline-twin-related reflection pair toward a reflection position of the other type: each albite- or pericline-twin component with a coherent boundary toward a missing component of the other type (A1↔(P1), A2↔(P2), or (A1)↔P1, (A2)↔P2) (Figs. 6e, 9c, 10e). [No diagram is shown for type (A1)↔P1, (A2)↔P2.] This type is transitional between the second one back and the next one. A possible explanation for this albite-twin pericline-transitional structure is based on the electron-microscope observations of Fitz Gerald & McLaren (1982; see also McLaren 1984, Fig. 9): it may represent a residual strained region between albite-twin domains and enveloping pericline-twin matrix, the latter now transformed into (fine) albite-twinned domains.

Streaks between each reflection of albite- and pericline-twin-related reflection pairs and a reflection of the other type: each albite- and pericline-twin component joined by coherent boundary to a component of the other type (A1↔P1, A2↔P2) (Figs. 9d, 10f). See Marfunin (1966, Fig. 27 right). A type of streaked-reflection photograph closely related to this has additional streaking between the two albite-twin reflections (Laves 1950, Plates 1F, 2E and Fig. 3). In our system of coding, it would be P1↔A1, A1↔A2, A2↔P2; its schematic representation would be a combination of those shown as Figures 10a and f.

Streaks between each reflection of albite- and pericline-twin-related reflection pairs and a reflection of the other type, and between albite-twin-related and orthoclase reflection triplets: each albite- and pericline-twin component joined by coherent boundary to a component of the other type, and each albite-twin component also joined by coherent boundary to a common orthoclase domain (P1↔*A1, A1*↔*O*↔*A2, A2*↔*P2) (Fig. 10g).* Other possible models for this type are shown by Laves (1950, Figs. 8A, B), and a precession example is given by Laves & Soldatos (1963, Fig. 4).

Interpretation from Precession Photographs of Albite Accompanying Microcline

The precession photographs of 25 of the 29 microcline specimens examined in this project show albite reflections, all of which give α^* values close to those for low albite, and all of which are very weak relative to corresponding reflections in microcline. The near-coincidence on the precession photographs of corresponding reciprocal axes of the two phases indicates that all our albite-containing microcline crystals are perthitic. All the photographs show actual coincidence of the *Y** axes of the two phases, the common situation, meaning that the two {010} structural planes are parallel. Furthermore, because the *b** values of the two feldspars are nearly the same (Table 4), their (0*k*0) reflections overlap. However, reciprocal period *a** of low albite is appreciably larger than for microcline, and because angle α^* for low albite departs appreciably from 90°, whereas γ^* does not (Table 4), the best resolution of reflections of both untwinned and albite- and pericline-twinned intergrown albite occurs on *X*-axis (0*kl*) precession photographs of microcline.

Structural information from α^*. The α^* parameter

projected along *Z*, and reciprocal lattice-points representing interpretations of possible types of *sharp* reflections on precession photographs. (Comparable diagrams for streaked reflections are given in Fig. 10.) The values given in a and b for the projected unit-cell parameters a', b', γ' are for maximum microcline, but in the drawing γ' is exaggerated to 80° for clarity. The orientations of the domains conform to those for the *Z*-axis reciprocal lattices and photographs in Figures 5 and 6. The labeling of the axes and reciprocal-lattice points shown in a, b and c also applies to the comparable cells in d, e and f. The distances of the reciprocal-lattice points ($h00_{A1}$, *etc.*) from any origin are arbitrary. (a) Albite-twinned microcline (Figs. 5d and 6d interpreted as unstreaked). (b) Pericline-twinned microcline (Figs. 5e and 6e interpreted as unstreaked). (c) Albite-twinned microcline plus orthoclase (Figs. 5b plus d; no recorded example). (d) Pericline-twinned microcline plus orthoclase (Figs. 5b plus e; no recorded example). (e) *M*-twinned microcline (Figs. 5f, g, 6f). (f) *M*-twinned microcline plus orthoclase (Figs. 5b plus f and g); [*e.g.*, Fig. 6–3a in Smith & Brown (1988) or Fig. 4 in Laves & Soldatos (1963), interpreted as unstreaked].

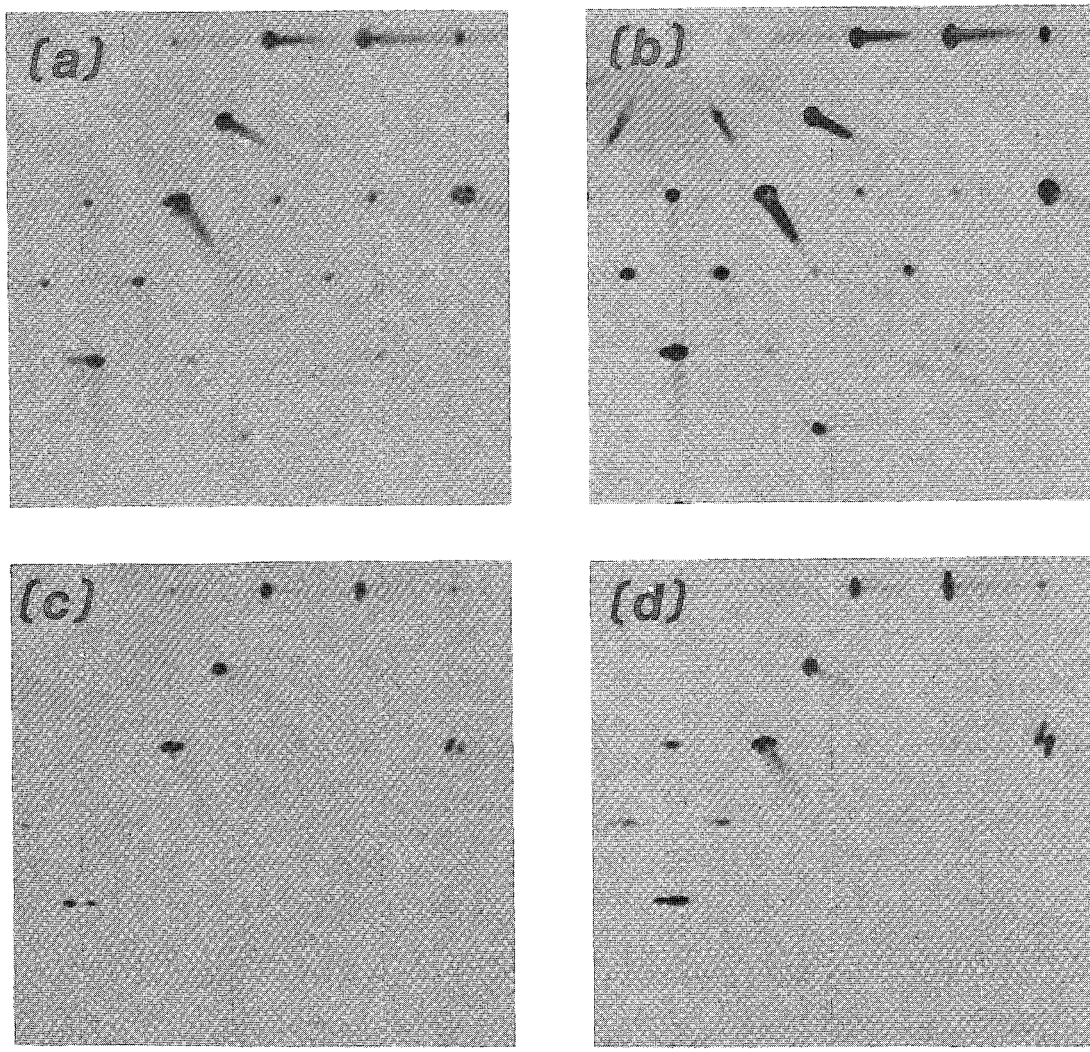

FIG. 9. *Z*-axis 0-level precession photographs (expanded by a factor of ~ 2.3) of microcline ± orthoclase representing some types of streaked reflections as explained in the text and in following Figure 10. Experimental conditions as for the 0-level photos in Figure 2. Orientations and hence labeling of the axes as in all other comparable photographs and reciprocal-lattice drawings, especially those in Figures 5, 6 and 8. (a) Albite-twinned maximum microcline, streaks A1 ↔ A2 (CG–03) (Fig. 10a). (b) Albite-twinned maximum microcline plus orthoclase, streaks A1 ↔ OR ↔ A2 (MLP/NZ–24) (Fig. 10c). (c) Albite-twinned microcline, streaks A1 ↔ (P1), A2 ↔ (P2) (SR-97) (see text and Fig. 10e). (d) *M*-twinned microcline, streaks A1 ↔ P1, A2 ↔ P2 (GPE–11) (see text and Fig. 10f).

alone cannot define either the structural state or composition, but it can suggest what these are. Relevant α^* values are: for low albite $An_{0.5}$ and high albite $An_{0.7}Or_{1.6}$, 86°20′ and 86°06′, respectively (Ribbe *et al.* 1969); for low plagioclase $An_{13.0}Or_{0.5}$, 86°13′ (Bambauer *et al.* 1967); and for heated plagioclase $An_{16.0}Or_{1.9}$, 86°01′ (Smith 1956). The α^* value of the albite in all but one of the grains examined in this project (McGregor 1984) is within 0.17° of 86.33° (= 86°20′) (Table 5). Considering that our error in angular measurement is, in general, 0.1°, the albite in these perthitic specimens may reasonably be interpreted to be close to end-member low albite both structurally and chemically.

Presence or absence of twinning. Albite may show the same four patterns of twinning, or an absence of twinning, as described earlier for microcline. The albite components in our 25 perthitic samples include

representatives of three of these types: five are untwinned, 18 are albite-twinned, and two are *M*-twinned; none is pericline-twinned only (Table 5, Fig. 11).

Evaluation of the proportion of albite in perthite and of the twin components. Three problems arise in these evaluations. The first stems from the fact that the albite is in such minor amounts that only its highest-intensity reflections appear, in which case the corresponding reflections of the K-feldspar are much too strong to be estimated on the photographs. Secondly, in our normal-exposure photographs, the albite reflections are too weak to be estimated, and longer exposures would simply have exacerbated the first problem. Thirdly, although albite and microcline are essentially isostructural, the chemical differences between them could result in appreciable differences in the structure factors of corresponding reflections of the two phases. As a result, we simply made visual estimations of the intensities of some corresponding albite and microcline reflections, from which we assigned rough volume percentages of albite of 1/2, 1, 2, or 3 (Table 5).

Comparison of Results of Powder Records with those of Precession Photographs

Powder-diffraction records were taken by the Gandolfi method for the same crystals examined by precession (~0.02 mg), and by diffractometer of a bulk pulverized sample (~25 mg) taken from the same specimen. It is possible for both types of powder record to provide (1) a general identification (microcline, low albite, orthoclase, *etc.*); (2) the triclinicity Δ of the K-feldspar; (3) refined unit-cell parameters (from which could be deduced the Al–Si distribution, composition, *etc.*); (4) presence of more than one K-feldspar; (5) presence or absence, and possibly the character, of the albite accompanying K-feldspar; and (6) indirect evidence for coherent interdomain boundaries.

Gandolfi photographs of representative single and multiphase crystals are included in McGregor (1984, Figs. 3–8 and 3–9), but they are not shown here because the significant details are difficult to reproduce; the photographs are like some of those shown by Goldsmith & Laves (1954, Figs. 3, 5 and 7), and have a general similarity to the Guinier photographs in Smith (1974, Fig. 6–17). Relevant parts of diffractograms of specimens representing particular features are, however, shown in Figure 11.

General identification

Both Gandolfi photographs (*e.g.*, those just referred to) and powder diffractograms (*e.g.*, Smith & Brown 1988, Figs. 6.7, 6.8, taken from Borg & Smith 1969) confirm the identification deduced by the precession technique.

Refined unit-cell parameters

Both powder methods can, in principle, provide a complete set of refined unit-cell parameters (*e.g.*, Stewart 1975, Ribbe 1983). This is a great advantage over the precession method, which permits the precise measurement of only α^* and γ^* ($\pm \sim 0.1°$). In practice, the relatively poor resolution and the width of the powder lines on Gandolfi photos preclude the collection of high-precision data. Powder diffractograms provide more precise raw data, and cell parameters from these data for the dominant phase in our 30 K-feldspar and two Na-feldspar specimens are given in McGregor (1984, Table 3–7). The reader must keep in mind that the results pertain to the bulk-powder specimen.

Triclinicity of the K-feldspars

Triclinicity values were derived from both the Gandolfi photos and the diffractograms. For sharp reflections and peaks, the error in Δ is, for a Gandolfi value, ~0.05, and that for one from a diffractogram, ~ 0.02. The former is about the same as that for a precession value (described above). For specimens that give broadened reflections or peaks on the powder record, precession values are, in general, more precise. The triclinicity values from the Gandolfi and diffractometer records for the specimens relevant to this paper are given, along with the precession values, in Table 5, where they have been extracted from the results for all our specimens given in McGregor (1984, Tables 3–6 and 3–9, respectively).

Broadened diffraction-maxima in powder records relative to streaked reflections in precession records

Line broadening in powder records results from a multiphase character of the specimen, or coherent interdomain boundaries between different phases or components of a twin, or to a combination of the two. In contrast to powder records, precession photographs reveal coherent boundaries as streaks between (usually) well-defined twin-related or multiphase reflections. Not only does the single-crystal record define the specific orientation of the streaking and, hence, of the coherent boundaries, but it may also permit a more precise measurement of the actual position of a reflection than does the powder record.

A comparison of the precession photograph with streaked reflections of a two-phase K-feldspar crystal consisting of albite-twinned maximum microcline plus orthoclase (Fig. 9b) with its powder diffractogram (Fig. 11e), along with the derived crystallographic data (Table 5), will serve to illustrate the superiority of the precession method over the powder method for such K-feldspar. For specimens that are single-phase but 'twin-streaked' (*e.g.*, Fig. 9d), the powder diffractogram (Fig. 11d) may, depend-

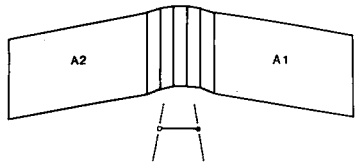

(a) A1⟷A2

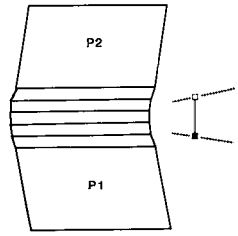

(b) P1⟷P2

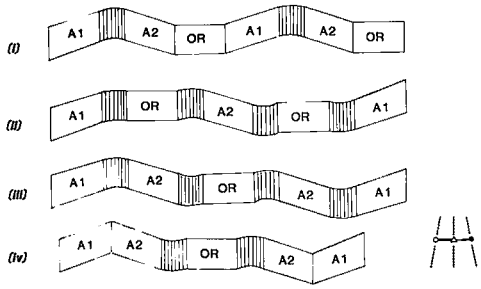

(c) A1⟷OR⟷A2

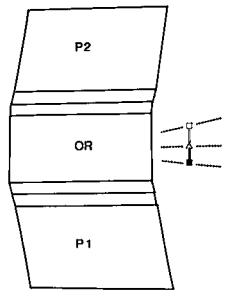

(d) P1⟷OR⟷P2

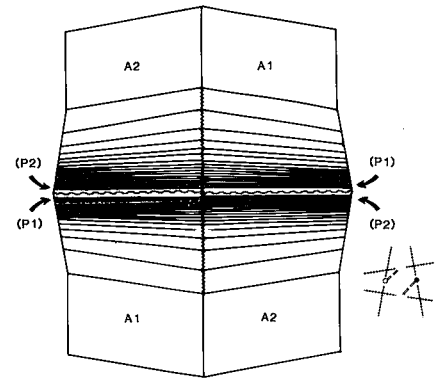

(e) A1⟷(P1), A2⟷(P2)

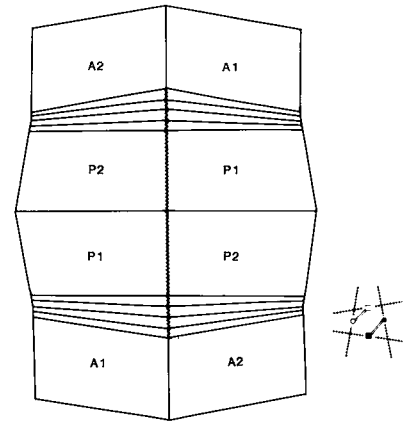

(f) A1⟷P1, A2⟷P2

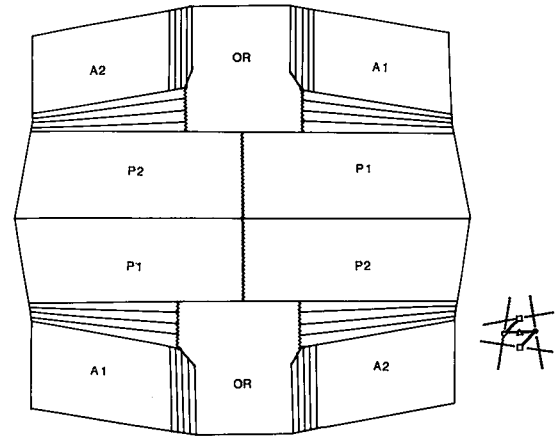

(g) P1⟷A1 , A1⟷OR⟷A2, A2⟷P2

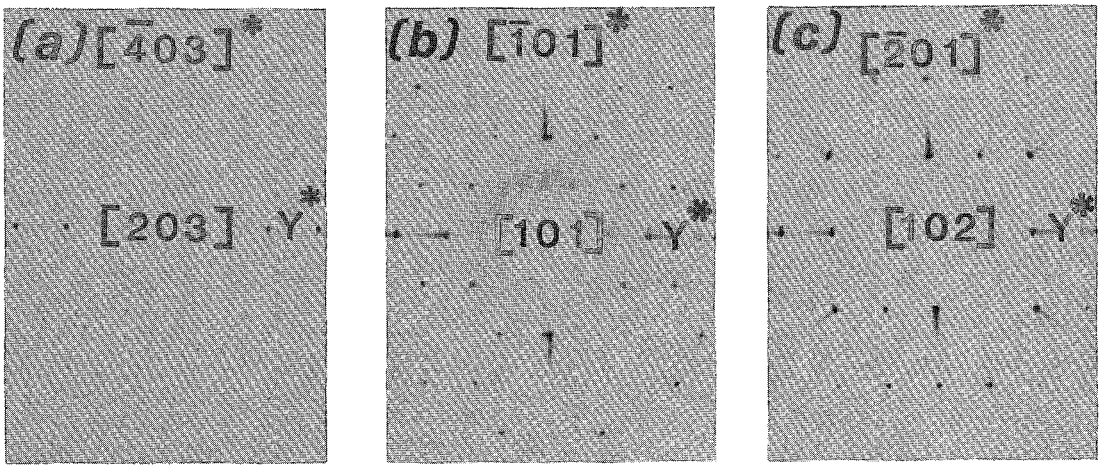

FIG. 11. *X*-axis 0-level precession photographs to scale of maximum microcline, showing minor untwinned, albite-twinned and *M*-twinned (low) albite. Arrows point to diagnostic albite reflections. Experimental conditions as for all other such photographs (*e.g.*, Fig. 2c). For photographs of low albite alone comparable to some of these, see Figure 7. The α^* angles of the minor albite in the three cases shown here correspond within the limits of error of $\pm$ 0.1° to that for low albite, 86.39° (Tables 4, 5). (a) Untwinned albite (AEC–20) (*cf.* Fig. 7b). Arrow points to 002. (b) Albite-twinned albite (CG–03). See Figure 7d for labeling of the axes. Arrows point to twinned pairs $00\bar{2}_{A1}$, $00\bar{2}_{A2}$. (c) *M*-twinned albite (SR–97). No comparable photo of albite alone, but labeling of the axes is deducible from Figures 11a and 7d. Arrows point to twinned pairs $00\bar{2}_{A1}$, $00\bar{2}_{A2}$, and 040_{P1}, 040_{P2}.

ing upon the extent of the streaking or broadening, give as precise numerical results (Table 5) as the precession photographs.

Albite in perthitic microcline

Both diffractograms and Gandolfi photographs of K-feldspar commonly reveal the presence of accompanying albite (Fig. 11f, and in Goldsmith & Laves 1954, Fig. 5a). The proportion of albite can be determined from photographs or diffractograms by measuring the intensity of certain reflections or peaks, respectively (*e.g.*, Ferguson & Ball 1987). Precession photos of a K-feldspar (Fig. 11) may give a clearer delineation of the albite reflections than the powder method (*cf.* Fig. 11b with Fig. 12f), and the precession method may therefore provide, in some cases, a more precise value for the proportion of albite in the microcline. Table 5 gives the proportions of albite in the microcline specimens relevant to this paper estimated from the precession and Gandolfi photographs and the diffractograms; these values are taken, respectively, from Tables 3–2, 3–6 and 3–9 in McGregor (1984).

CONCLUSIONS

This description of the application of the precession technique to alkali feldspar should facilitate the systematic examination of rock suites in order to elucidate the detailed characteristics ('fine structure') not available by powder methods. However, one needs to address the following questions before proceeding to the petrogenetic interpretations. (1) How representative are the features observed for one tiny (~ 0.2 mm) crystal? An examination of several crystals from a given specimen and from a given rock mass will be required to assess the internal con-

FIG. 10. Simplified diagrammatic 2-dimensional models of the direct lattices of maximum microcline and orthoclase projected along *Z*, and reciprocal-lattice points representing interpretations of possible types of *streaked* reflections on precession photographs. Diagrams comparable to those for sharp reflections shown in Figure 8; the description, the legend and the labeling of the axes and reciprocal-lattice points also apply here. Figures 10a–d, f, g correspond to Figures 8a–d, e, f, respectively. (a) Albite-twinned microcline, A1 ↔ A2 (Fig. 9a). (b) Pericline-twinned microcline P1 ↔ P2. (c) Albite-twinned microcline plus orthoclase, A1 ↔ OR ↔ A2 (Fig. 9b). Four possible configurations are shown. (d) Pericline-twinned microcline plus orthoclase, P1 ↔ OR ↔ P2. As in c several configurations are possible, but only the one corresponding to c(ii) is shown. (e) Albite-twinned microcline, A1 ↔ (P1), A2 ↔ (P2) (Fig. 9c). This type is transitional between those in Figures 8a and 10f. (f) *M*-twinned microcline, A1 ↔ P1, A2 ↔ P2 (Fig. 9d). (g) *M*-twinned microcline plus orthoclase, P1 ↔ A1, A1 ↔ OR ↔ A2, A2 ↔ P2. One of several possible configurations.

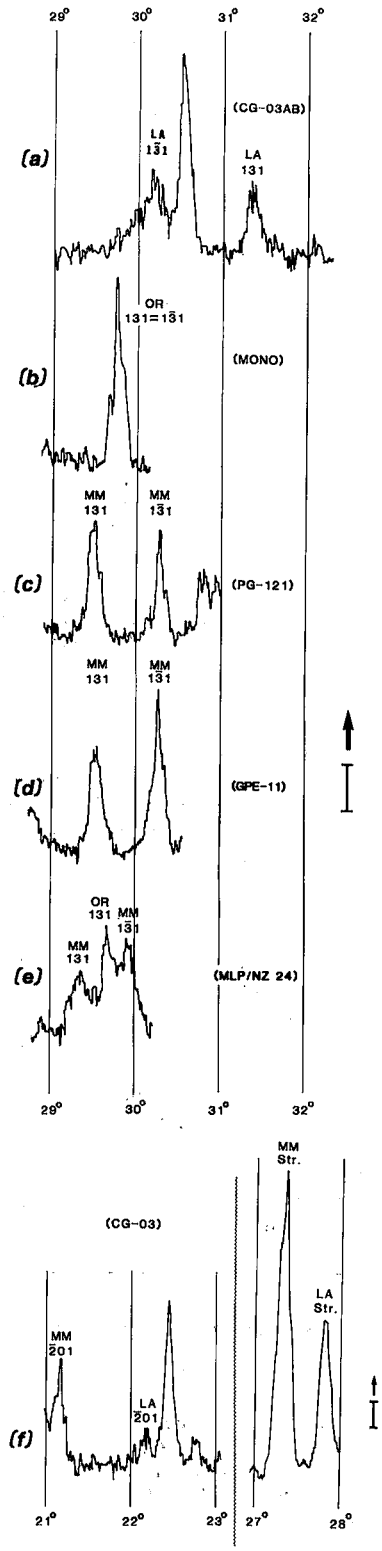

sistency of the results. (2) What are the implications, in terms of 'fine structure', of the streaks on the precession photographs? The answers can probably be provided only by combined selected-area electron diffraction (SAD) and transmission electron microscopy (TEM), which provide photographs of areas on a submicroscopic scale subjected to electron diffraction. The examination of several crystals by the precession technique *and* SAD–TEM is necessary to provide interpretations of all the precession effects in terms of microstructure. (3) What is the origin of the twins and microstructures that are deduced from the precession photographs? The generally accepted concept of Laves (1952), that *M*-twinning in microcline can arise only from the inversion of a monoclinic precursor, is consistent with SAD-TEM observations (*e.g.*, McLaren 1984, Parsons & Brown 1984). However, the petrogenetic significance of most fine structural features revealed by the precession method will probably become clear only when answers have been provided to questions (1) and (2) above, and when this technique has been applied to several K-feldspar crystals, well-characterized petrologically and geochemically, in combination with optical, electron-microprobe and, preferably, SAD–TEM techniques.

The authors intend to consider some of these matters in a subsequent paper, which will focus on the two suites of granitic and pegmatitic K-feldspar from Manitoba and Ontario (McGregor 1984) that were briefly introduced early in the paper.

Acknowledgements

The authors express their gratitude to the following individuals for help with this research and the preparation of this paper. Petr Černý provided all our microcline and albite specimens and much background material on them, and on those of Elias Ucakuwun. Dr. Černý also gave us much valuable professional advice, as did Frank C. Hawthorne.

FIG. 12. Diagnostic portions of powder diffractograms of maximum microcline (MM), orthoclase (OR) and low albite (LA) illustrating various effects related to the precession photographs described below and in the text. Radiation Ni-filtered Cu$K\alpha$, scan speed 0.25° 2θ/min., chart speed 20 mm/°2θ, recorder full scale 2000 c.p.s., time constant 2 s. Labeled peaks are diagnostic. Intensity I is on an arbitrary scale. Figures given below refer to the corresponding precession photographs. Further information from specimen numbers in Tables 1, 2 and 5. (a) LA (Figs. 7b, f). (b) OR (Fig. 6b). (c) MM, sharp precession-reflections (Fig. 6c). (d) MM, streaked precession-reflections (Fig. 9d). (e) MM plus OR, streaked precession-reflections (Fig. 9b). (f) MM plus LA, unstreaked MM–LA precession-reflections (Figs. 9a, 11b).

Essential technical assistance was provided by N. A. Ball, I. Berta, R. Chapman, S. Fay, A. Flynn, R. E. Meintzer and R. Pryhitko. C.R.M. thanks Marilyn Armstrong and especially the following members of her family for various kinds of technical assistance and for prolonged encouragement and support: Josef J. Macek, Frances Jill McGregor, and Frank and Elaine McGregor. The authors also thank Lowell T. Trembath and an anonymous referee for valuable constructive criticisms, and especially Robert F. Martin for infinite patience while making innumerable invaluable improvements to the manuscript. The Manitoba Department of Energy & Mines has provided C.R.M. with time and facilities, and the Natural Sciences and Engineering Research Council of Canada has made this research possible by grants to R.B.F.

References

Azaroff, L.V. (1968): *Elements of X-ray Crystallography*. McGraw-Hill, New York.

Bambauer, H.U., Eberhard, E. & Viswanathan, K. (1967): The lattice constants and related parameters of 'plagioclases (low)'. *Schweiz. Mineral. Petrogr. Mitt.* **47**, 351-364.

Borg, I.Y. & Smith, D.K. (1969): Calculated X-ray powder patterns for silicate minerals. *Geol. Soc. Am. Mem.* **122**.

Buerger, M.J. (1964): *The Precession Method in X-Ray Crystallography*. Wiley, New York.

Ferguson, R.B. & Ball, N.A. (1987): Quantitative phase analysis of Rb-enriched maximum microcline and low albite by X-ray powder diffractometry. *Can. Mineral.* **25**, 337-345.

Fitz Gerald, J.D. & McLaren, A.C. (1982): The microstructures of microcline from some granitic rocks and pegmatites. *Contrib. Mineral. Petrol.* **80**, 219-229.

Goldsmith, J.R. & Laves, F. (1954): The microcline–sanidine stability relations. *Geochim. Cosmochim. Acta* **5**, 1-19.

Henry, N.F.M., Lipson, H. & Wooster, W.A. (1960): *The Interpretation of X-ray Diffraction Photographs (2nd ed.)*. Macmillan, New York.

Hovis, G.L. (1986): Behavior of alkali feldspars: crystallographic properties and characterization of composition and Al–Si distribution. *Am. Mineral.* **71**, 869-890.

Kaneko, K. (1974): Simple method of alkali-feldspar separation from granitic rocks for X-ray diffractometry. *Miy. Daig. Kyoi. Kiyo, Shizen Kagaku,* **35**, 1-5 (in Japanese; in *Chem. Abstr.* **81**, 155684x).

Kroll, H. & Ribbe, P.H. (1987): Determining (Al,Si) distribution and strain in alkali feldspars using lattice parameters and diffraction-peak positions: a review. *Am. Mineral.* **72**, 491-506.

Laves, F. (1950): The lattice and twinning of microcline and other potash feldspars. *J. Geol.* **58**, 548-571.

_____ (1952): Phase relations of the alkali feldspars. I. Introductory remarks. *J. Geol.* **60**, 436-450.

_____ & Goldsmith, J.R. (1961): Polymorphism, order, disorder, diffusion and confusion in the feldspars. *Cursillos y Conferencias, Inst. Luca Mallada VIII*, 71-80.

_____ & Soldatos, K. (1962): Über "verzerrte" Mikroklin-Verzwillingung und über unsymmetrische Albitausscheidung in Kryptoperthit. *Z. Kristallogr.* **117**, 209-217.

_____ & _____ (1963): Die Albit/Mikroklin-Orientierungs-Beziehungen in Mikroklinperthiten und deren genetische Deutung. *Z. Kristallogr.* **118**, 69-102.

Marfunin, A.S. (1966): *The Feldspars: Phase Relations, Optical Properties, and Geological Distribution*. Israel Prog. Sci. Translations, Jerusalem.

McGregor, C.R. (1984): *Characterization of Granitic and Pegmatitic K-Feldspars from Lac du Bonnet, Southeastern Manitoba and Dryden, Northwestern Ontario by Rapid X-Ray Diffraction and Chemical Methods*. M.Sc. thesis, Univ. Manitoba, Winnipeg, Manitoba.

McLaren, A.C. (1984): Transmission electron microscope investigations of the microstructures of microclines. *In* Feldspars and Feldspathoids (W.L. Brown, ed.). Proc. NATO Adv. Study Inst., Reidel, Dordrecht, The Netherlands (373-409).

Nuffield, E.W. (1966): *X-Ray Diffraction Methods*. Wiley, New York.

Parsons, I. & Brown, W.L. (1984): Feldspars and the thermal history of igneous rocks. *In* Feldspars and Feldspathoids (W.L. Brown, ed.). Proc. NATO Adv. Study Inst., Reidel, Dordrecht, The Netherlands (317-371).

Ribbe, P.H. (1983): Aluminum-silicon order in feldspars; domain textures and diffraction patterns. *In* Feldspar Mineralogy (2nd edition; P.H. Ribbe, ed.). *Mineral. Soc. Am., Rev., Mineral.* **2**, 21-55.

_____, Megaw, H.D. & Taylor, W.H. (1969): The albite structures. *Acta Crystallogr.* **B25**, 1503-1518.

Smith, J.V. (1956): The powder patterns and lattice parameters of plagioclase feldspars. I. The soda-rich plagioclases. *Mineral. Mag.* **31**, 47-68.

——— (1974): *Feldspar Minerals. 1. Crystal Structure and Physical Properties.* Springer-Verlag, Berlin.

——— & BROWN, W.L. (1988) *Feldspar Minerals. 1. Crystal Structures, Physical, Chemical, and Microtextural Properties (2n ed.).* Springer-Verlag, Berlin.

SOLDATOS, K. (1962): Ueber die kryptoperthitische Albit-Ausscheidung in Mikroklinperthiten. *Nor. Geol. Tidsskr.* **42(2)**, 180-192.

STEWART, D.B. (1975): Least squares refinement program for unit cell parameters. *In* Feldspar Mineralogy (P.H. Ribbe, ed.). *Mineral. Soc. Am., Rev. Mineral. 2.* A1-A6 (Appendix).

TUTTLE, O.F. (1952): Optical studies on alkali feldspars. *Am. J. Sci. Bowen Vol.,* 553-567.

UCAKUWUN, E.K. (1981): *The Pegmatites and Granitoid rocks of the Dryden Area, Northwestern Ontario.* M.Sc. thesis, Univ. Manitoba, Winnipeg, Manitoba.

VAN DER PLAS, L. (1966): *The Identification of Detrital Feldspars.* Elsevier, Amsterdam.

Received May 19, 1987, revised manuscript accepted March 1, 1989.